Journal of Volcanology and Geothermal Research 401 (2020) 106973

Contents lists available at ScienceDirect

Journal of Volcanology and Geothermal Research

journal homepage: www.elsevier.com/locate/jvolgeores

A Miocene Phreatoplinian eruption in the North-Eastern Pannonian Basin, Hungary: The Jató Member

Tamás Biró [a,*], Mátyás Hencz [a], Károly Németh [b], Dávid Karátson [a], Emő Márton [c], Alexandru Szakács [d,e], Balázs Bradák [f], Zoltán Szalai [g,h], Zoltán Pécskay [i], István János Kovács [j]

[a] Eötvös University, Faculty of Science, Department of Physical Geography, Pázmány Péter sétány 1/C, H-1117 Budapest, Hungary
[b] Massey University, School of Agriculture and Environment, Private Bag 11 222, Palmerston North 4442, New Zealand
[c] Mining and Geological Survey of Hungary, Paleomagnetic Laboratory, Homonna str. 9., H-1118 Budapest, Hungary
[d] Romanian Academy, Institute of Geodynamics, Dept. of Endogene Processes, Natural Hazard and Risk, 19-21 Jean-Louis Calderon St., R-020032, Bucharest-37, Romania
[e] Sapientia University, Department of Environmental Sciences, Calea Turzii nr. 4., 400193 Cluj-Napoca, Romania
[f] Burgos University, Paleomagnetic Laboratory, Department of Physics, Av. de Cantabria, s/n, 09006 Burgos, Spain
[g] Research Center for Astronomy and Earth Sciences, Geographical Institute, Budaörsi str. 45, (MTA Research Building), H-1112 Budapest, Hungary
[h] Eötvös University, Faculty of Science, Department of Environmental and Landscape Geography, Pázmány Péter sétány 1/C, H-1117 Budapest, Hungary
[i] Institute of Nuclear Research (ATOMKI), Isotope Climatology and Environmental Research Centre (ICER), K-Ar Group, Bem tér 18/c, H-4026 Debrecen, Hungary
[j] Research Center for Astronomy and Earth Sciences, Lendület Pannon LitH$_2$Oscope Research Group, Csatkai Endre u. 6-8, H-9400 Sopron, Hungary

ARTICLE INFO

Article history:
Received 13 November 2019
Received in revised form 10 June 2020
Accepted 10 June 2020
Available online 19 June 2020

Keywords:
Silicic hydrovolcanism
Accretionary lapilli
Dry-to-wet transition
Miocene
Bükk Foreland Volcanic Area
Carpatho-Pannonian region

ABSTRACT

A Middle Miocene, ~8 m thick pyroclastic succession, reported from the Bükk Foreland Volcanic Area (BFVA) in Northern Hungary (Central Europe) specified here as the Jató Member, was produced by silicic phreatomagmatism (Phreatoplinian sensu *lato*). Two well-preserved outcrops ~8 km apart and inferred to be within ~10–50 km from source represent the discontinuously exposed, layered, paleosol-bounded, phreatomagmatic Jató Member. They show an identical phenocrystal assemblage of feldspar, biotite and amphibole without weathered zones or signs of erosion, that suggest deposition in one eruption phase lasting hours to months. The succession contains three subunits: 1) subunit A, 1.8 m thick, a series of well-sorted fine to coarse ash or lapilli tuff layers with constant thickness; 2) subunit B, 2.1 m thick, a series of normal-graded layers with an upper fine-grained zone containing abundant ash aggregates with a coarser-grained core and distinctively finer-grained outer rim; 3) subunit C, 4.5 m thick, a massive, poorly to well-sorted coarse ash with gas escape structures and ash aggregates at its base. The upward change of these lithofacies implies an initially sustained dry fallout-dominated deposition of ash and pumice lapilli resulting in subunit A. Subsequently, multiple wet and dilute Pyroclastic Density Currents (PDCs) dispersed subunits B and C. The general abundance of PDC-related ash aggregates in the middle-upper part of the succession (particularly in subunit B), and the transformation of a fall-dominated to a collapsing depositional regime producing wet dilute PDCs, imply the increasing influence of water during the eruption (Phreatoplinian sensu *lato*). The presence of water is related to an epicontinental sea during Middle to Late Miocene in the Carpatho-Pannonian region. The transition from an initial dry magmatic phase generated fallout activity followed by the emplacement of wet PDCs' rich in ash aggregates, when external water infiltrated from a surrounding lake or sea water entered the vent.

1. Introduction

Phreatomagmatism occurs when hot magma of any type comes into contact with external water explosively (Morrissey et al., 2000). Phreatomagmatism, while commonly used as synonym for hydrovolcanism, is recently more specifically referred to explosive volcanism resulting from molten-coolant interaction (MFCI) processes typically in subaerial conditions (Németh and Kósik, 2020). There are well-documented Late Quaternary pyroclastic formations that show signs of interaction between silicic magma and a significant body of external water: the Hatepe and Rotongaio ashes of the AD 183 Taupo Eruption in New Zealand (Walker, 1981a), the 25.4 ka Oruanui Formation of the Taupo Volcano (Self and Sparks, 1978; Self, 1983; Wilson, 2001), the ~70 ka Neapolitan Yellow Tuff from the Campi Flegrei caldera in Italy (Cole and Scarpati, 1993), the 161 ka Kos Plateau Tuff from the Eastern Aegean (Allen and Cas, 1998), and the Askja AD 1875 layer C (Sparks et al., 1981). The expression "phreatoplinian", based on fallout tephra dispersal and grade of fragmentation, was applied to silicic eruptions that result in pyroclast deposition to the same or even larger areal

* Corresponding author.
E-mail address: birotamas@caesar.elte.hu (T. Biró).

https://doi.org/10.1016/j.jvolgeores.2020.106973

extent than Plinian ones (>500 km^2), showing a high degree of fragmentation reaching a scaled value of over 70% (Self and Sparks, 1978; Houghton et al., 2015a). Phreatoplinian tephras show less characteristic change of granulometric parameters with distance from vent than Plinian ones (Walker, 1981a) and their total grain-size distribution show poor sorting due to common ash accretion and contemporaneous fallout with larger pumice clasts (Walker, 1981a; Sparks et al., 1981).

In practice, total grain-size distribution, change in granulometric parameters with distance from vent, and D-F (dispersal versus fragmentation) values for ancient, poorly exposed pyroclastic layers are not easy to determine due to the common scarcity of suitable outcrops and the difficulty of identifying and correlating single fallout layers that can be linked to the same explosive event. The phreatomagmatic origin of ancient tephra could be deduced from 1) the textural features of pyroclasts that can be associated to the presence of water at the vent causing quench fragmentation, and 2) the identification of sedimentological features caused by water vapour in the eruption column and/or water in the deposited tephra. In this way, a typical phreatomagmatic tephra can be distinguished on the basis of i) the significant amount of fine ash (sensu *lato*) (McPhie, 1986); ii) the abundance of ash aggregates and fine ash coating on larger pyroclasts (coarse ash to lapilli) (Wilson, 2001; Ellis and Branney, 2010); iii) the associated fine-grained, non-welded pyroclastic density current (PDC) deposits which commonly contain plant remains (Porreca et al., 2008); iv) the characteristically angular and blocky ash particles (Scarpati et al., 1993; Ellis and Branney, 2010) showing solidity and convexity values dominantly between 0.8 and 1.0 (Liu et al., 2015); and v) the presence of diatoms, incorporated from external water, that came into contact with hot silicate melt (Van Eaton et al., 2013). For example, the phreatomagmatic origin of the Late Carboniferous Cana Creek Tuff (Australia; McPhie, 1986), the Ordovician Whorneyside Tuff (English Lake District; Branney, 1991) and the Miocene Deadeye Member (Snake River Plain, USA; Ellis and Branney, 2010) were determined by recognizing some of the features listed above. However, during several silicic eruptions, external surface water came into contact with the magma after partial or complete volatile exsolution; e.g. after initial magmatic fragmentation (Self, 1983; Houghton et al., 2015a, 2015b; White and Valentine, 2016) and only ~30% of the resulting glass fragments in the ash fraction show particle shape signatures related to water-induced quench fragmentation (e.g. MFCI; Büttner et al., 2002). Consequently, determining the phreatomagmatic origin (sensu stricto) for ancient silicic successions is a real challenge. Revealing water influence on a silicic eruption in the geological past thus requires careful investigation of the entire succession recording continuous presence of water in the eruption column and the aggrading pyroclastic layers. We use the term Phreatoplinian sensu lato (with capital 'p') to describe deposits with evidence for large-scale interaction of magma and external water, but lacking sufficient field exposure or data to plot on a Walker dispersal-fragmentation classification diagram (Walker, 1973).

During the Early and Middle Miocene (Szabó et al., 1992; Pécskay et al., 1995, 2006) widespread silicic explosive volcanism took place in the intrabasinal part of the Carpatho-Pannonian region (CPR; Fig. 1a) in present-day Eastern-Central Europe in several episodes (Szabó et al., 1992; Pécskay et al., 2006). Related pyroclastic rocks cover at least 50,000 km^2 based on qualitative areal estimates (Pantó, 1965; Ravasz, 1987). The average cumulative thickness of the Early to Middle Miocene silicic pyroclastic rocks was estimated at ~90 m by considering several thousand boreholes, suggesting a ca. 4500 km^3 total bulk volume estimate (Lukács et al., 2018). The long timespan and the large volume are comparable with pyroclastic rocks from ignimbrite flare-up episodes caused by high mantle flux (0–10 Ma; 10^3–10^4 km^3; Gravley et al., 2016 and references therein). The largest exposed occurrence of the silicic pyroclastic rocks in the CPR is the Bükk Foreland Volcanic Area (BFVA). Here, on an area of ca. 8 × 40 km, a ~ 200 m thick pyroclastic succession crops out (Szakács et al., 1998).

In this paper, we present a detailed physical volcanological description of a bedded, fine-grained unit with abundant ash aggregates from the BFVA, specified as the Jató Member, that was deposited ~14.9 Ma ago according to zircon U—Pb dating (Lukács et al., 2015, 2018), in a subaerial setting. The general abundance of PDC-related ash aggregates in the middle to upper part of the succession, and the transformation of a fall-dominated to a collapsing depositional regime producing wet ignimbrites imply abruptly intervening water influence on a silicic eruption (Phreatoplinian sensu *lato*).

2. Geological background

Eastward drift and counterclockwise rotation of two microplates (Alcapa and Tisza-Dácia) into the "Carpathian embayment" of the CPR during Late Oligocene to Early-Middle Miocene times induced large-scale normal faulting and crustal thinning related to strong extension (Csontos et al., 1992; Márton and Fodor, 1995, 2003; Márton and Márton, 1996; Márton et al., 2007). The extension induced decompression melting in the asthenosphere and the lithospheric mantle, which was previously enriched by subduction-related metasomatism (Szabó et al., 1992; Konečný et al., 2002; Seghedi et al., 2004; Harangi and Lenkey, 2007; Kovács and Szabó, 2008). Magmatism at the surface resulted in generation of volcanic edifices such as intermediate (mostly andesitic) groups of lava domes and composite volcanoes (e.g.: Central Slovakian Volcanic Field, Visegrád Mountains, Börzsöny Mountains; Konečný et al., 1995, Karátson et al., 2000, 2007), and silicic explosive volcanism-related ignimbrite fields in the intrabasinal part of the CPR (Fig. 1a) during the Early and Middle Miocene, i.e. from ~21 Ma to ~12 Ma on the basis of extensive K—Ar dating (Pécskay et al., 1995, 2006).

The Early and Middle Miocene silicic pyroclastic successions, up to few hundreds of metres thick, were penetrated by boreholes in Southern Transdanubia, the Great Hungarian Plain, the Transcarpathian Basin and the Transylvanian Basin under a pile of Neogene to Quaternary siliciclastic deposits which may reach up to 4000 m in thickness (Széky-Fux et al., 1987; Zelenka et al., 2004) including salt in the Transylvanian Basin (Szakács et al., 2012). Scattered surface occurrences are also known in several areas, including the Börzsöny and Cserhát Mountains, the southern and northern foreland of the Mátra and Bükk Mountains, the Eperjes-Tokaj Mountains, the Mecsek and the Transylvanian Basin (Fig. 1a; Pantó, 1962; Hámor et al., 1979; Szabó et al., 1992; Zelenka et al., 2004; Szakács et al., 2012). The largest and most complex surface representation of these pyroclastic rocks is found in the Bükk Foreland Volcanic Area (BFVA; Fig. 1b) covering an area of at least 320 km^2. The oldest dated ignimbrite in the BFVA gave a 20.40 ± 1.72 Ma biotite K/Ar age (Márton and Pécskay, 1998). The Harsány Ignimbrite, which is found at the top of the BFVA sequence and considered the youngest pyroclastic succession by Lukács et al. (2015), yielded an age of 15.66 ± 0.66 Ma by whole rock K/Ar dating (Márton and Pécskay, 1998) and 13.35 ± 1.01 Ma by biotite K/Ar dating (Lukács et al., 2007), while U/Pb dating on zircons yielded 14.358 ± 0.015 Ma. New zircon U/Pb ages from the entire succession of BFVA suggests an age range of the volcanism from ~18.2 to 14.4 Ma (Lukács et al., 2018).

The pyroclastic rocks cropping out in the BFVA are dominantly composed of thick ignimbrites with non-welded, slightly- to densely-welded facies interbedded, and/or capped by thin pyroclastic fall deposits commonly associated with locally thick, valley-confined reworked tephras between the major ignimbrite units (Fig. 2; Capaccioni et al., 1995; Szakács et al., 1998). The five known voluminous ignimbrite units of BFVA (at least 20 m thick each) are, in chronological order, the Eger Ignimbrite, Mangó Ignimbrite, Bogács Ignimbrite, Demjén Ignimbrite and Harsány Ignimbrite (Lukács et al., 2018 and references therein). Paleomagnetic declination results, radiometric ages, lithological features and phenocryst assemblages of these major ignimbrites are summarized in Fig. 2.

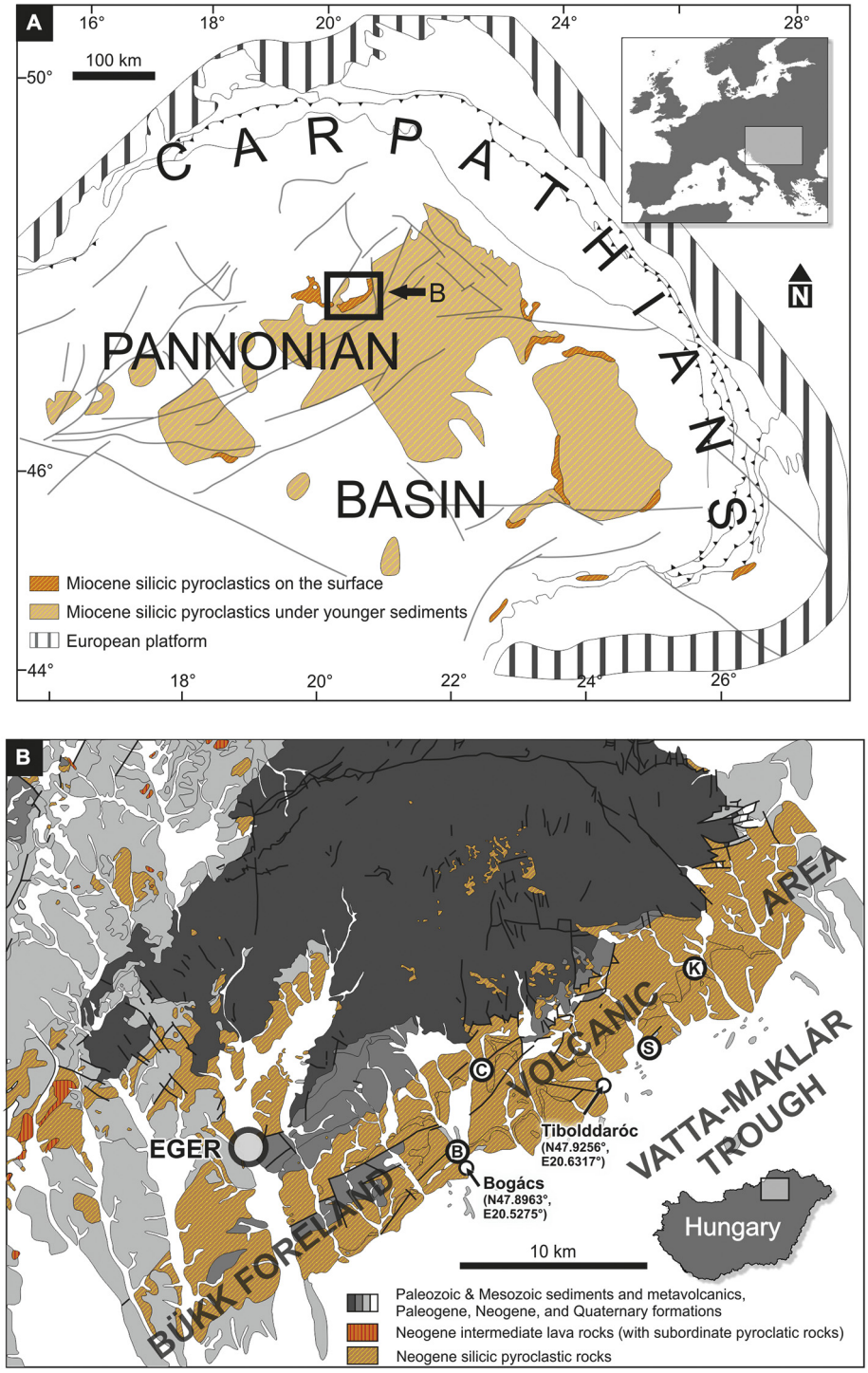

Fig. 1. Regional geological setting (a) and volcanological map (b) of the Bükk Foreland Volcanic Area with the studied Bogács and Tibolddaróc sites marked. a) Areal distribution of Miocene silicic pyroclastics in the Carpathian-Pannonian Region. The black rectangle with "B" marks the location of the Bükk Foreland Volcanic Area. The map was modified after Szakács et al. (2018). b) Volcanological map of the Bükk Foreland Volcanic Area. Basemap: 1:100.000 geological map of Hungary, published by the Mining and Geological Survey of Hungary (https://map.mbfsz.gov.hu/fdt100/). Exact location of the Bogács and Tibolddaróc sampling sites is specified with WGS84 geographic coordinates. Sampling sites of Szakács et al. (1998): B – Bogács-Abandoned quarry; C – Cserépfalu; S – Sály; K – Kisgyőr-Kőbánya-tető.

The location of source vents for various BFVA pyroclastic successions is unknown. However, qualitative or semiquantitative interpretations based on various investigations implied multiple source areas, that are located in the Vatta-Maklár Trough at the southern margin of the Bükk Mountains (Fig. 1b): Directional magnetic fabric of the Bogács ignimbrite indicated a source region south of Tibolddaróc (Szakács et al., 1998). Pyroclast transport direction indicators and the direction of grain-size coarsening from the Lower Tuff Complex point towards the southwest from Eger (Fig. 1b; Szakács et al., 1998). The eastward thickening of the Lower Tuff Complex ignimbrites and the Harsány Ignimbrite obtained from borehole data shows an eastern source region (Lukács et al., 2010). Lateral facies variations in the Demjén Ignimbrite are consistent with a source region close to the southwestern margin of the BFVA (Lukács et al., 2015).

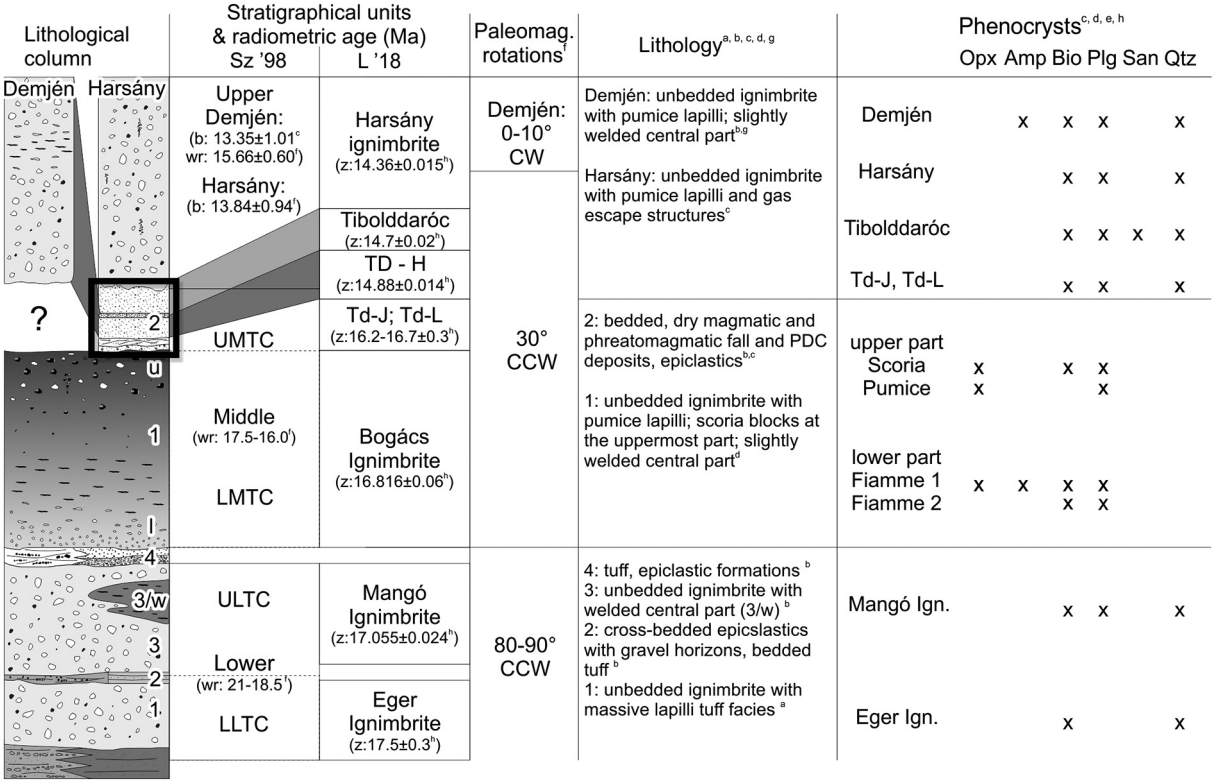

Fig. 2. Lithological, stratigraphic, petrographic, geochronological and paleomagnetic features of the main pyroclastic complexes in the BFVA. Unit thicknesses are not to scale. The investigated Tibolddaróc Succession was deposited between the Bogács and Harsány Ignimbrite units and marked with a black rectangle. Sz '98 – Szakács et al. (1998), L '18 – Lukács et al. (2018). Types of radiometric age determinations: b – K/Ar age of biotite; wr – K/Ar age of whole rock; z – zircon U/Pb ages. Source of data: a – Capaccioni et al. (1995); b – Szakács et al. (1998); c – Lukács et al. (2007); d – Czuppon et al. (2012); e – Póka et al. (1998); f – Márton and Pécskay (1998); g – Lukács et al. (2015); h – Lukács et al. (2018). Opx – orthopyroxene; Amp – amphibole; Bio – biotite; Plg – plagioclase; San – sanidine; Qtz – quartz.

This study focuses on a complex, bedded pyroclastic succession described as the Tibolddaróc Succession (Lukács et al., 2007, 2015), found between the Bogács and Harsány Ignimbrites (Fig. 2). Szakács et al. (1998) documented the basic physical volcanological features of the Tibolddaróc Succession using field volcanology data from exposures at the settlements of Bogács, Cserépfalu, Tibolddaróc, Sály and Kisgyőr-Kőbányatető (Fig. 1b) and argued the succession is a phreatomagmatic pyroclastic complex with abundant ash aggregates. Later, a more detailed field observation on the succession at the settlement of Tibolddaróc (Fig. 1b) allowed distinguishing 11 units (layer B-L; Lukács et al., 2007): four pyroclastic fall deposits with 0.2–0.5 m thickness, from which Td-L is produced by phreatomagmatic fallout, three ignimbrites with 15, 1 and 0.5 m thicknesses, and four reworked volcaniclastic layers, respectively. Zircon U/Pb ages of Td-L (16.7 ± 0.25 Ma), Td-J (16.2 ± 0.30 Ma), Td-H (14.88 ± 0.20 Ma), and Td-E, F (14.65 ± 0.20 Ma) from Tibolddaróc imply quiescence periods as long as 0.3–1.2 Ma between the dated units (Lukács et al., 2015), characterized by the formation of epiclastic deposits.

In this study a detailed description on the best-preserved part of the Tibolddaróc Succession is given, which is shown to be produced by silicic phreatomagmatism and designated here as the Jató Member. The term "Jató" is borrowed from Jató Hill near Bogács village, because the best-preserved occurrence of the studied unit crops out on the eastern flank of that hill.

3. Materials and methods

3.1. Field description

Basic physical volcanological features of each individual pyroclastic bed, such as thickness, bedform, sorting, grain-size characteristics, colour and contact details were recorded on the field in the vicinity of the two localities (Figs. 3, 4). The best exposures are known near the village of Bogács and Tibolddaróc (Fig. 1b). Detailed description was only possible for a particular ~8.5 m part of the succession (mentioned above; for details see Section 4.2), because other units are heavily weathered.

3.2. Granulometry

To understand the grain-size distribution, indicative of transport mode of the pyroclasts in each subunit of the Jató Member, 33 samples were analysed (Fig. 5). Standard granulometric methodology was applied: dry sieving and laser diffraction particle sizing in order to compute median grain size and sorting coefficient of Inman (1952) and F2 parameter of Walker (1983). Detailed description of granulometric analyses is provided in the Appendix. Granulometry also helped to segregate individual pyroclasts for further textural and chemical investigations. Eleven samples from subunit A, seven from subunit B and four from subunit C were investigated from Bogács. In addition, eight samples from subunit A, one from subunit B and two from subunit C were investigated from Tibolddaróc. Thus, comparison between the same layers from Bogács and Tibolddaróc was possible across eight well-defined layers. Granulometric analyses were performed only on those layers which are friable or poorly cemented.

3.3. Anisotropy of magnetic susceptibility

Magnetic susceptibility is the induced magnetic moment of a substance if an outer magnetic field is applied. Anisotropy of magnetic susceptibility (AMS) measures the orientation of magnetic carriers in a rock. AMS therefore is a widely used technique to investigate the

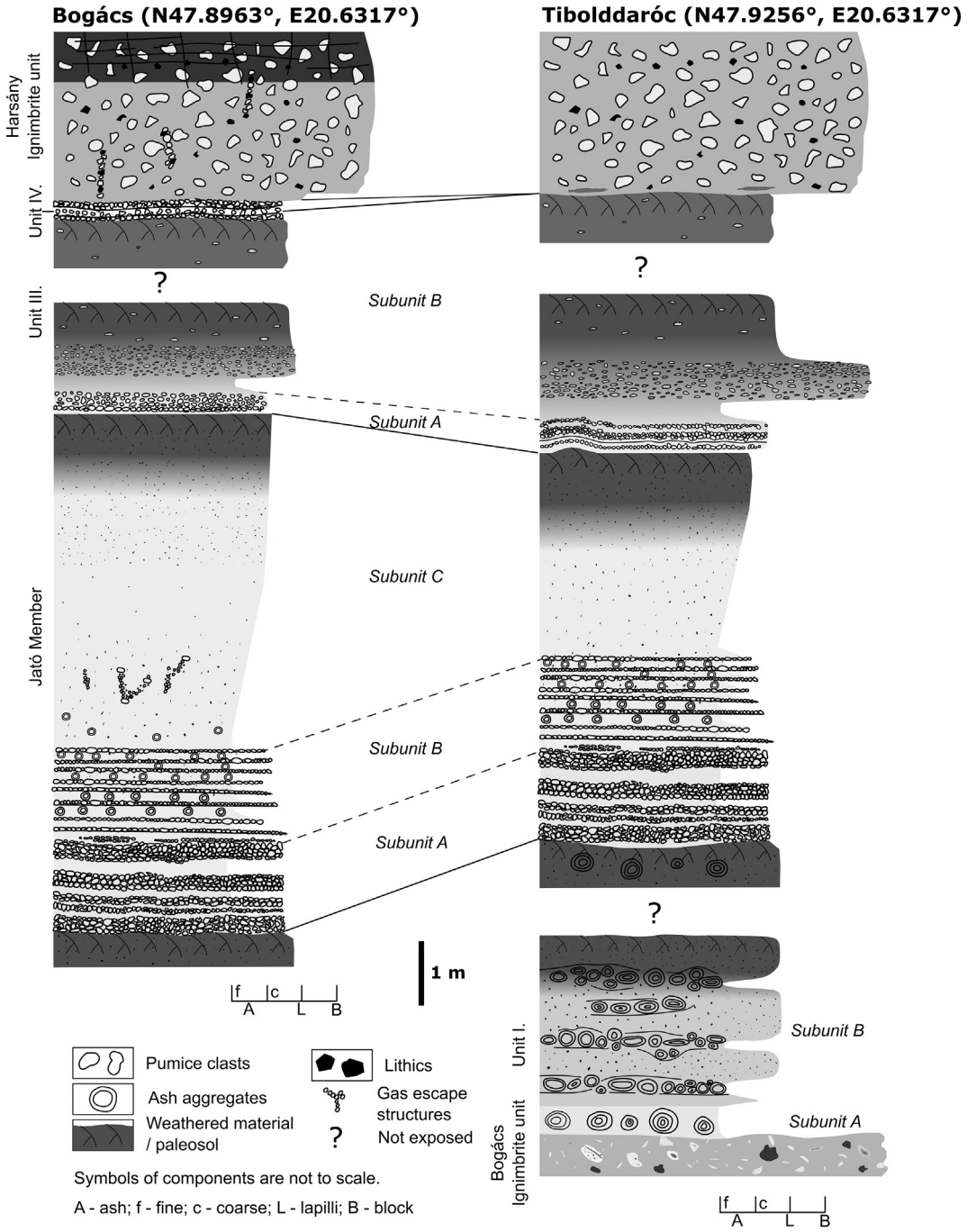

Fig. 3. Lithological features of the pyroclastic succession at Bogács and Tibolddaróc. The succession contains four units (I-IV) at Bogács and three units (I-III) at Tibolddaróc. Unit IV is absent at Tibolddaróc. Only the uppermost part of unit I is cropping out at Bogács. The two occurrences of the Jató Member and Unit III can be readily correlated. Only the Jató Member is not effected by heavy weathering. The thickness of the Harsány Ignimbrite unit is not to scale at Tibolddaróc.

magnetic fabric of various rocks (Rochette et al., 1992). AMS can be described as a triaxial ellipsoid with K_{max} being the maximum, K_{int} the intermediate and K_{min} the minimum susceptibilities. AMS is routinely used for pyroclastic density current deposits to determine flow directions and depositional processes (Cañón-Tapia and Mendoza-Borunda, 2014; Ort et al., 2015). In this study, AMS is used to obtain information on the amount of shearing during pyroclast deposition, then to decide whether a layer is emplaced by pyroclast fallout or by pyroclastic density current. Forty-eight standard cylindrical samples were drilled in the field for AMS measurements at Bogács from the following layers: layer 13 of subunit A, layer 2 and 4 from subunit B, and three samples from the base and top of subunit C. Samples were recovered from two sites from subunit C: from ~1 m above its base, and from below the weathered zone at the top of this subunit (Fig. 5). Details of the AMS measurements and corresponding statistical treatment are presented in the Appendix.

4. Results

4.1. Units of the Tibolddaróc Succession

In this study, the stratigraphy and physical volcanological features of the layered Tibolddaróc Succession, which was deposited in between the Bogács and Harsány Ignimbrite units, were examined at the village

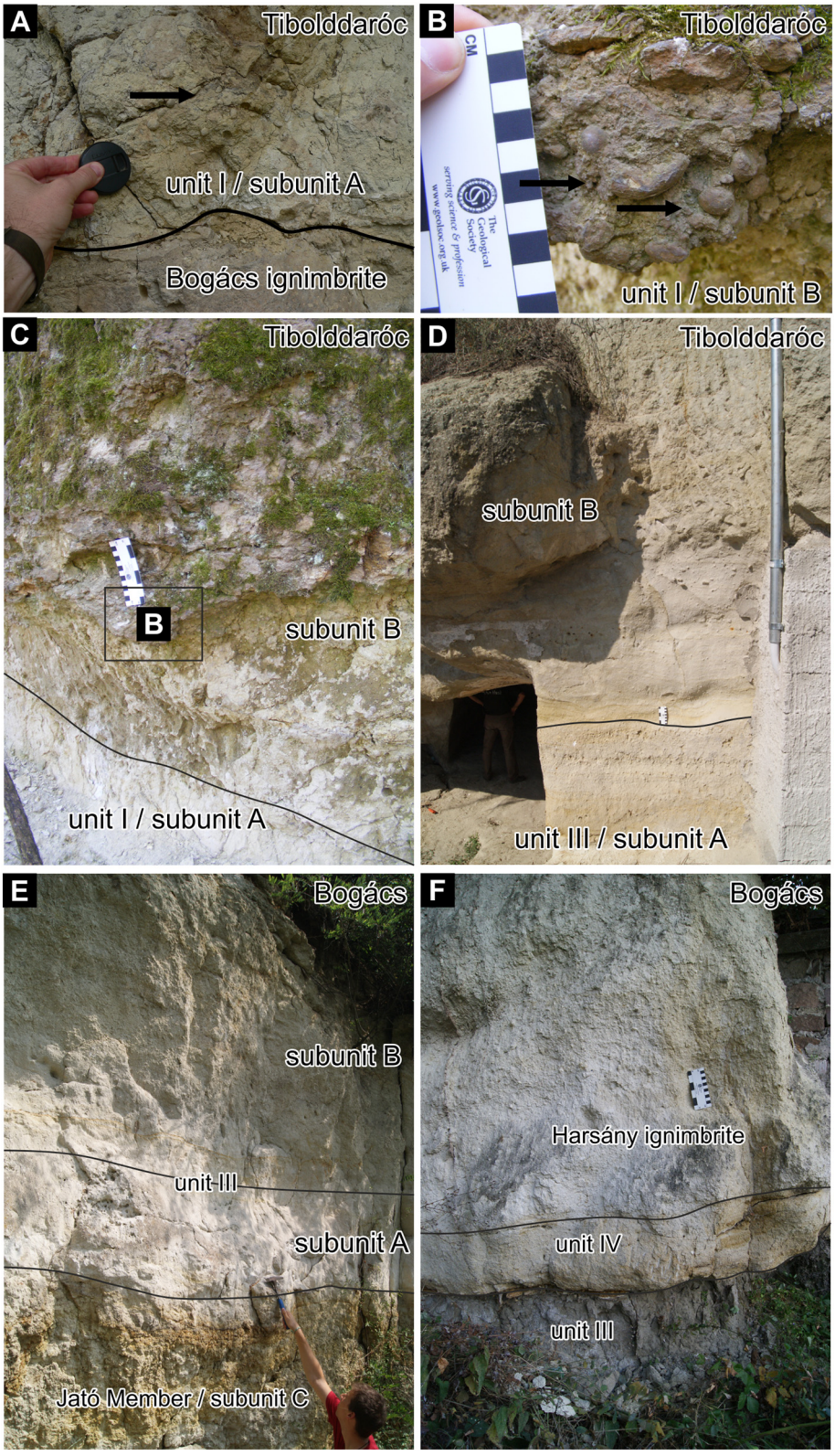

Fig. 4. Field appearance of Unit I, III and IV. A – The boundary between the Bogács ignimbrite and subunit A of Unit I at Tibolddaróc. Arrow points to an ash aggregate; B – Ash aggregates in subunit B of Unit I at Tibolddaróc; C – Unit I at Tibolddaróc, note the location of ash aggregate rich zone on picture B; D – Unit III at Tibolddaróc; E – Unit III at Bogács; F – Unit IV and the Harsány ignimbrite at Bogács.

of Bogács and Tibolddaróc (Fig. 1b) located 8.6 km apart. Other occurrences of the Tibolddaróc Succession at Bogács – an abandoned quarry, Sály, Kisgyőr – Kőbányatető (Fig. 1b) mentioned by Szakács et al. (1998) are heavily weathered; individual beds cannot be confidently distinguished; hence we have not found them suitable for detailed macro- and microtextural analysis. The succession has slightly different overall thickness at the two localities, ~14.5 m at Bogács and ~13 m at Tibolddaróc, respectively. As a result of field mapping and vertical

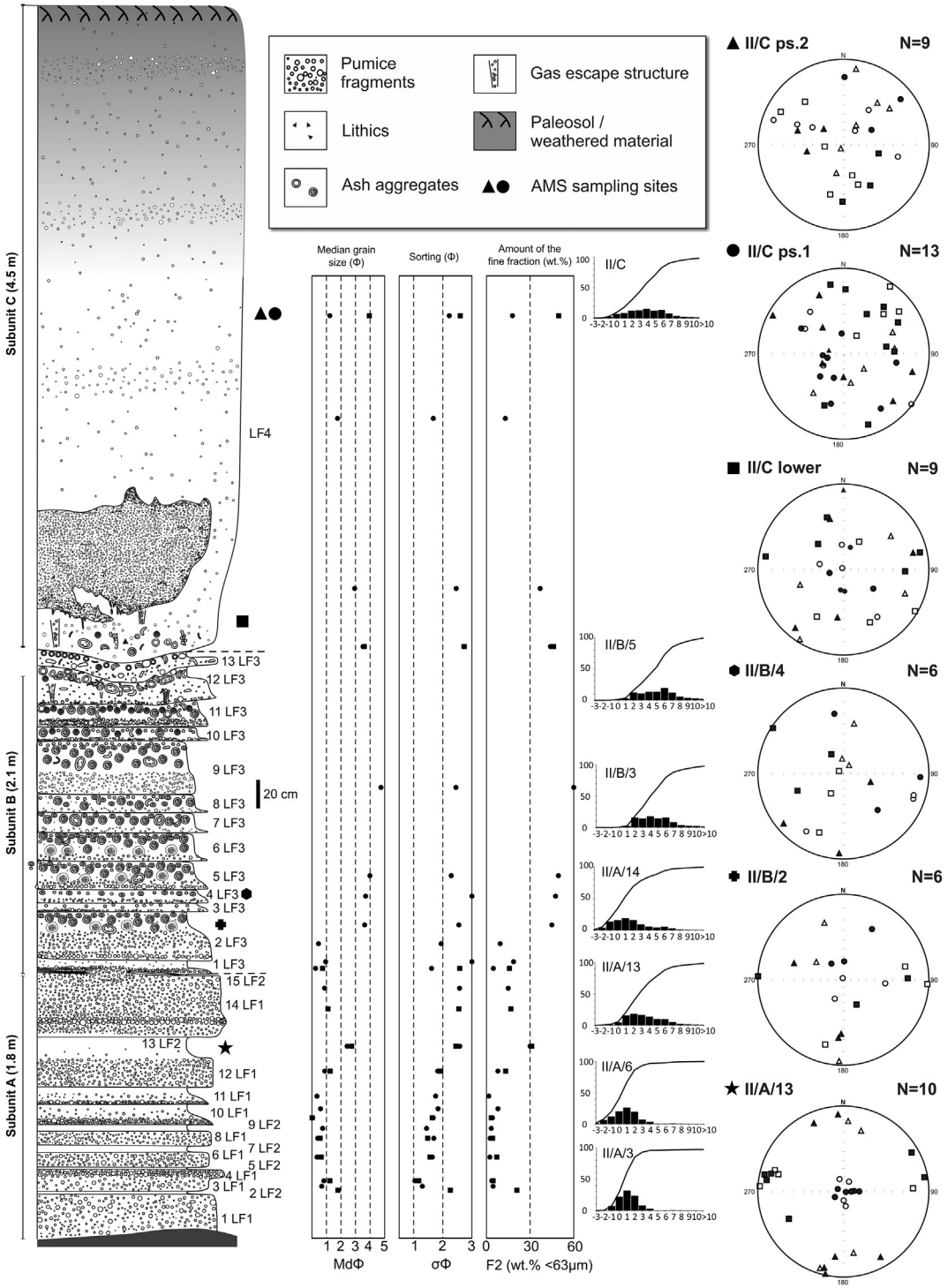

Fig. 5. Detailed stratigraphic log, granulometry and magnetic fabric of the Jató Member. Mdϕ and $\sigma\phi$ are the median grain size and the Inman (1952) sorting parameter, respectively in ϕ units ($\phi = -\log_2 d$, where d is the grain diameter in mm). F2 is the amount of the <1/16 mm (<0.063 mm) fraction, expressed in weight percent (Walker, 1983). Symbols: circles – samples from Bogács; squares – samples from Tibolddaróc. Black symbols mark the positions of samples collected for AMS measurements. Stereoplots: square – K_{max}, triangle – K_{int}, circle – K_{min}, open symbols mark samples, where the F-test was negative. See the Appendix for further details. LF is lithofacies; see chapter 4 and Table 2 for further discussion.

sectioning, four lithostratigraphic units have been distinguished from base to top labelled as unit I, unit II (i.e. the Jató Member), unit III and unit IV, respectively, based on bedding characteristics, average grain-size and colour (Figs. 3, 4, 5). The boundaries between the units are laterally continuous, clearly visible and sharp. Unit IV is only exposed at Bogács and it is unclear that at Tibolddaróc it has ever existed and/or it has been eroded. The lower and upper parts of the succession (units I, III and IV) are weathered, thus their original bedding and granulometry could not be determined in the field. Sedimentological features of the identified units are summarized in Table 1.

4.2. Field and grain-size characteristics of the Jató Member (unit II)

As summarized in Table 1, the Jató Member has been subdivided into three subunits (subunit A, B and C; Figs. 3, 5). In more detail, four lithofacies (LF1–4 hereafter) can be discriminated based on thickness,

grain-size characteristics and abundance of ash aggregates (Table 2). The full granulometrical dataset is available in the Electronic Supplementary Material. There is a successive change of dominant LF: Subunit A consists of 15 layers, from which layer 1, 3, 4, 6, 8, 10, 11, 12, 14 representing LF1 (Table 2). It is a well-sorted tuff or lapilli tuff with typical Mdφ between 0 and 1 (0.5–1.0 mm) and variable sorting (σφ is between 1 and 2.5). The grain-size distribution curve of LF1 is characterized by a normal peak centered around 0.5 mm (φ = 1). Constant thickness of LF1 layers are observed in the several m^2 to several 10 m^2-sized, scattered outcrops Six layers, namely layer 2, 5, 7, 9, 13, 15 occur in subunit A representing LF2 (Fig. 6), which is a moderately sorted fine tuff often containing pumice lapilli characterized by Mdφ between 2 and 3 (0.25–0.125 mm), and σφ of 2–3. A smaller symmetric peak in the grain-size distribution is present at φ = 6 (0.016 mm) besides the main peak at φ = 2 (0.25 mm). The thickness of LF2 varies from layer to layer between 1 and 20 cm. LF1 and 2 layers are distributed nearly homogeneously in subunit A, i.e. there is no part of subunit A, where LF2 layers are more frequent.

The layers of subunit B have a uniform, characteristic appearance: each consists of a coarser-grained lower part with median grain size between 0.5 and 1 mm (Mdφ: 0.3–0.5) and moderate sorting (σφ: 1.61 and 1.93) overlain by a fine-grained upper part with median grain size between 0.5 and 0.1 mm (Mdφ: 1–3.7) and poor sorting (σφ ~3), containing very abundant ash aggregates (Table 2). These layers are designated as LF3 in our interpretative schema (Fig. 7a, b). Except for the lowermost layer in subunit B, all layers defined as LF3 contain ash aggregates in the upper, relatively fine-grained part. In this paper 'ash aggregate' describes all types of ash aggregates, regardless their internal structure. Most ash aggregates in LF3 show a relatively coarse-grained core and a fine-grained rim defining a layered structure. The grain-size distribution of cores and rims of ash aggregates was not measured in this study. However, contrasting grain-size of the coarser cores and relatively fine-grained rims is evident to the naked eye (Fig. 7c, d, e). The abundance and size of ash aggregates show a general gradational pattern in LF3. Just above the lower, coarser part, sparse, usually 4–10 mm-sized ash aggregates are typical. In this zone, ash aggregates show weak clustering rather than homogeneous distribution. Towards the top of the layer, the size of ash aggregates decreases (down to 1–2 mm in diameter); on the contrary, their abundance increases (Fig. 7c). The 3–10 cm thick uppermost zone of the layers is composed entirely of ~2 mm-sized ash aggregates. Most of the ash aggregates show spherical geometry. Rarely, especially the >0.5 cm-sized ash aggregates are deformed, showing an ellipsoid-like contour in cross section (Fig. 7e). Rarely, the core of ash aggregates is occupied by a 2–3 mm large feldspar phenocryst or lithic clast. In layer 7 some ash aggregates with 1–1.5 cm diameter show a more complex internal structure than the typical coarse core-fine rim type observed in LF3. Such ash aggregates show variation of relatively fine-grained and coarser-grained concentric layers. This is the only layer where this type was observed.

Above subunit B, a diffusely-bedded, 4.5 m thick tuff with abundant gas escape structures is noted, designated as subunit C and LF4 (Table 2, Fig. 8). Subunit C shows slight upward coarsening of median grain size at Bogács: 0.1 mm (Mdφ = 3.5) at its base, 0.13 mm (Mdφ = 3) at 1 m above its base, 0.3 mm (Mdφ = 1.7) in the middle part and 0.45 mm (Mdφ = 1.2) below the weathered zone. The deposit sorting, expressed in σφ is between 1.7 and 2.4. Two peaks at 0.015 mm (φ = 6), and 0.5 mm (φ = 1), result in a bimodal grain-size distribution.

Layer 3, 6, 8, 10, 12, 13, 14 from subunit A, layer 1 from subunit B, and subunit C were sampled for granulometrical analyses both at Bogács and at Tibolddaróc. Most of these layers show almost identical granulometry features (Fig. 5, Electronic Supplementary Material). Different σϕ values characterize only the lower part of layer 1 in subunit B at the two outcrops, namely, σϕ is 1.61 at Bogács and 2.56 at Tibolddaróc, but Mdϕ values are similar, 0.26 and 0.70, respectively. By contrast, both the Mdϕ and σϕ values are different (1.2 and 4.0, and 2.2 and 2.6, resp.) below the weathered top of subunit C in the

Table 1
Characteristics of the Tibolddaróc Succession.

Unit	Description	Interpretation
IV	Thickness: shows laterally changes in the outcrop; maximum: 0.5 m. Structure: well-sorted coarse tuff and lapilli tuff layers with laterally variable thickness. Average diameter of pumice clasts: 0.5 cm and never exceeds 1 cm.	Fall deposits
III	*Thickness*: ~4 m at Bogács and ~ 5 m at Tibolddaróc. Its overall thickness can only be determined with uncertainty, because the outcrops are not continuous laterally. *Structure*: two subunits (subunit A and B). The internal structure and grain-size characteristics of unit III are different at Bogács and Tibolddaróc. *Subunit A*: the lowermost 26 cm thick layer of subunit A at Tibolddaróc is a very fine yellowish white tuff with faint bedding. Above this layer the remaining 94 cm part of subunit A is a series of coarse well-sorted tuff layers 3–20 cm thick each containing cm-sized dense pumice clasts, grey, banded lithic clasts and mm-sized quartz, feldspar and biotite crystals. Maximum diameter of pumice clasts: 5 cm (average of the three biggest pumice clast). Lithics are much rarer than pumice clasts and have a maximum diameter of 1.5 cm. Quartz, feldspar and biotite crystal fragments with 3 mm diameter are presented. At Bogács, the lowermost fine tuff is ~15 cm thick. Similarly, the coarser-grained upper part is just ~50 cm thick here, and finer-grained than at Tibolddaróc. *Subunit B*: gradational lower contact; only the lowermost 1.5 m thick part of this subunit can be investigated. The upper ~3 m thick part of Subunit B has a lower porosity and much higher clay content than its lower part, suggesting weathering. The lowermost layer of subunit B is a ~ 40 cm thick, fine grained, poorly sorted tuff with rare ~1 cm-sized pumice clasts at both occurrences. Above that layer, a ~ 0.5 m thick poorly sorted layer with abundant cm-sized pumices developed. The maximum size of pumice clasts is 3 cm at Bogács and 6 cm at Tibolddaróc. After that, a fine-grained, poorly sorted layer was deposited, which becomes denser and clay-rich gradually upwards.	Subunit A: fall deposits Subunit B: PDC deposits +/− fall deposits
Jató Member (II)	*Thickness* is different at the two localities: ~8 m at Bogács and 7 m at Tibolddaróc. *Structure*: three subunits (subunit A, B and C). *Subunit A*: 1.8 m thick at both localities. It mainly consists of the alternation of coarse tuff layers, 2–20 cm thick and lapilli tuff layers, up to 40 cm thick, with laterally constant thickness at outcrop scale. The sorting of individual layers are good. *Subunit B*: 2.1 m thick at both sites, consists of layers with a uniform internal structure. The basal part is a coarse-grained tuff, whereas the upper part is fine-grained and contains abundant ash aggregates. *Subunit C*: 4.5 m thick at Bogács and 3 m thick at Tibolddaróc, is a massive lapilli tuff with 2 cm maximum pumice diameter. Minor grain-size variations indicate only diffuse bedding in the subunit. At the lowermost 1 m thick part it contains abundant ash aggregates and gas escape structures. The uppermost 2 m thick part is heavily weathered, it is clay-rich, and much less porous than the lower parts. The colour of	Subunit A: fall deposits Subunit B: wet PDC deposits Subunit C: wet ignimbrite

Table 1 (*continued*)

Unit	Description	Interpretation
I	the weathered part gradually transforms upwards from light grey into dark grey. All the layers contain abundant feldspar, biotite, amphibole and sparse quartz phenocrysts. *Thickness*: ~3 m at Tibolddaróc. Only the uppermost 0.5 m is exposed at Bogács. *Structure*: ~0.5 m thick basal subunit (subunit A), which directly overlies the Bogács Ignimbrite, and a ~2.5 m thick upper subunit (subunit B; Fig. 3). *Subunit A*: well-sorted, very fine-grained light grey fine tuff, 0.5 m thick and containing abundant cm-sized ash aggregates. Its thickness is constant laterally. The largest ash aggregate reaches 3 cm in diameter. *Subunit B*: 2.5 m thick, poorly-sorted, yellowish grey, heavily altered tuff. Two types of layers: i) dark-grey, fine grained, hardly compacted tuff with abundant deformed, flattened ash aggregates; the thickness of these layers is changing laterally between 3 and 15 cm in places showing faint cross-bedding features; ii) light brown poorly-sorted ~60–70 cm thick layers with mm-sized pumice clasts; ash aggregates within the tuff are up to 1 cm in diameter and often flattened. The uppermost ~1 m thick part of unit I is heavily weathered.	Subunit A: phreatomagmatic fall deposit Subunit B: wet PDC deposits

two outcrops (Figs. 3, 5; note the different thickness of subunit C at Bogács and Tibolddaróc).

4.3. Anisotropy of magnetic susceptibility

The mean magnetic susceptibilities of the investigated samples from the Jató Member are weak, ranging between 35 and 100 × 10^{-6} SI (Fig. 9a). Most of the samples have <70 × 10^{-6} SI mean magnetic susceptibility. Samples from the lower part of subunit C have slightly higher magnetic susceptibilities (80–100 × 10^{-6} SI) considering the studied samples. The P′ of the investigated samples are also weak (generally lower than 0.5%). Only three samples show P′ values higher than 1%. It is important however, that P′ is independent of the mean magnetic susceptibility (Km; Fig. 9a). All layers show significant scatter of the ellipsoid shape parameter ($-1 < T < 0.8$; Fig. 9b). The F-test value of 24 out of the 53 investigated sample is <3.4817, which implies statistically isotropic magnetic fabric for 45% of the samples.

The distribution anisotropy of principal susceptibilities is generally poor (Fig. 5, 9b). The orientation of the principal susceptibility axes is generally chaotic, except in layer 13 of subunit A and in layer 2 of subunit B. In the former, all three axes are grouped (Fig. 5), and K_{min} axes are vertical, K_{max} axes are W-E oriented and consequently the K_{int} axes are oriented in N-S direction. In layer 2 of subunit B, Kmax axes are also aligned in the W-E direction, but the other two axes are intermixed.

5. Discussion

5.1. Deposition from multiple eruption phases at subaerial setting recorded in the Tibolddaróc Succession

Four main units are identified within the Tibolddaróc Succession. Detailed field logging of the two occurrences at Bogács and Tibolddaróc has shown that the two outcrops, located 8.6 km apart, consist of the same pyroclastic units. Consequently, the existence of the same, dominantly fine-grained pyroclastic units at both sites imply explosive eruptions that caused tephra deposition over an area of at least 10^2–10^3 km^2.

Weathered zones occur at the top of unit I, III and the Jató Member which display a transitional lower contact, indicating that the fresh tephra of each unit incrementally weathered towards the top of the units (Figs. 3, 6c, 8c). The upper contacts of the weathered zones are sharp and irregular. The presence of weathered zones at the upper part of the eruptive units is a common feature of pyroclastic successions aggraded during discrete volcanic phases separated by long quiescence periods (on the order of 10^2–10^5 years) associated with intense surface weathering and soil formation (e.g. Santorini: Vespa et al., 2006; Taupo Volcanic Zone: Wilson, 1993; Vesuvius: Vogel et al., 2016). A lowermost fine accretionary lapilli-bearing tuff (Td-L), a fine tuff (Td-J), a lapilli-bearing poorly-sorted tuff (Td-H), and a bedded sequence consisting of fine to coarse tuff layers (Td-E, F) separated by reworked volcaniclastic layers were described at Tibolddaróc (Lukács et al., 2007, 2015). However, both the lithostratigraphy and the genetic interpretation of Lukács et al. (2015) differ from what is suggested in this work. Nevertheless, Td-L (in Lukács et al., 2015) can be tentatively identified as subunit A of unit I in our division; Td-J and the overlying volcaniclastics to subunit B of unit I in our division; Td-H and the volcaniclastics on its top to the Jató Member; and Td-E, F and overlying volcaniclastics to unit III. Zircon U/Pb ages of Td-L (16.7 ± 0.30 Ma), Td-J (16.2 ± 0.30 Ma), Td-H (14.88 ± 0.014 Ma), and Td-E, F (14.7 ± 0.20 Ma; Lukács et al., 2015) from Tibolddaróc imply quiescence periods as long as 0.3–1.2 Ma between the dated units. The inferred long periods of volcanic quiescence between the emplacement of the units and the warm and humid climate reconstructed for the Middle Miocene (Jiménez-Moreno et al., 2005) suggest intense paleosol formation in the volcanic quiescence periods. Reconstructed average annual paleo temperature was 18–20 °C and the average annual paleo precipitation was 1400–1200 mm for the Badenian stage (corresponding to Langhian and most of Serravallian in standard chronostratigraphy), based on the palynological analysis of Tengelic 2 borehole (Jiménez-Moreno et al., 2005) located in Southern Transdanubia, 200 km away from Bogács to the southwest. Consequently, the presence of 2–3 m thick paleosols at the top of separate pyroclastic successions indicate, that at Bogács and Tibolddaróc localities there was a subaerial environment in the Middle Miocene, where pyroclast deposition occurred during multiple eruption phases. In the Middle Miocene, an incremental transgression from SE towards NE from 16.3 to 13.4 Ma was reconstructed (Kovács et al., 2007), which resulted in an archipelago with large areas covered by shallow sea and 10^2–10^3 km^2 large land patches (Kovács et al., 2007; Kováč et al., 2017). The Bükk Mts. and their vicinity might have been subaerial terrains (Bérczi et al., 1988; Szakács et al., 1998; Kováč et al., 2017) according to the presence of sediments from terrestrial environments. The presence of paleosols in the Tibolddaróc Succession confirms these former paleoenvironmental reconstructions.

The heavy weathering of unit I and III hinders their genetic interpretation. To interpret lithofacies and draw an eruption scenario is only possible for the Jató Member, the subject of this study, which shows the characteristics of an explosive eruption influenced by external water.

5.2. The Jató Member

5.2.1. Fingerprints of phreatomagmatism in ancient pyroclastic successions

Determination of the main type of a volcanic eruption from a pyroclastic deposit can be based on thickness and grain-size data collected in a number of spatially distributed outcrops. In optimal circumstances, the total grain-size distribution can be calculated (Walker, 1981a) and the data can be plotted on the dispersal (D) versus fragmentation (F) diagram by interpolating isopach lines (Walker, 1973). The area covered by a typical phreatoplinian fall deposit overlaps with the area covered by plinian fall deposits generated from “dry”, magmatic eruptions;

Table 2
Features of various lithofacies in the Jató Member.

Lithofacies	Description	Layers	Representative grain-size distribution curve	Interpretation
LF1	*Thickness*: 4–35 cm. *Lithology*: well-sorted coarse tuff, rich in pumice clasts (>80 wt% in general), showing sharp but non-erosive contacts; thickness is laterally constant at an outcrop scale; components: pumice clasts, biotite, feldspar and subordinate amount of amphibole and small lithics (<5%). *Granulometry*: Md ϕ: generally <1 (on average, 0.5 mm); sorting: variable, ranging between 1 and 2.5; F2: generally <10 wt%. *Grain-size distribution*: dominated by a normal peak at $\phi = 1$ (0.5 mm). The grain-size distribution of layer 14, a ~35 cm thick coarse tuff, shows a second but very moderate peak of fine ash at 6 ϕ (0.016 mm).	Layer 1, 3, 4, 6, 8, 10, 11, 12, 14 in subunit A	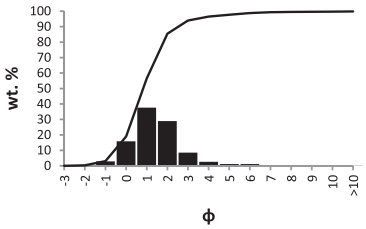	Fall deposit
LF2	*Thickness*: 1–20 cm. *Lithology*: fine tuff with sharp but non-erosive or, sometimes, diffuse lower contact; components: fine glass shards, pumice fragments and phenocrysts (>80), larger, 1–3 mm-sized pumice clasts, lithics and biotite fragments are rare (<20 wt%). *Granulometry*: Md ϕ and $\sigma\phi$: between 2 and 3; F2: 30 wt%; *Grain-size distribution*: a smaller symmetric peak in the grain-size distribution is present at $\phi = 6$ (0.016 mm) besides the main peak at $\phi = 2$ (0.25 mm).	Layer 2, 5, 7, 9, 13, 15 in subunit A	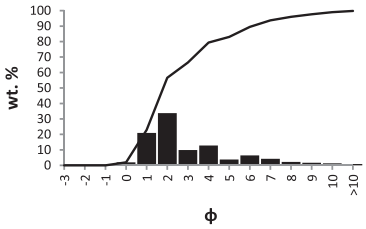	PDC deposit from low-energy, dilute currents
LF3	*Thickness*: 5–40 cm. *Lithology*: normal graded coarse to very fine tuff, consisting of a relatively coarser basal part and a fine-grained upper part often bearing abundant ash aggregates ('ash aggregate' describes all types of ash aggregates, regardless its internal structure); contact between the coarser basal part and the upper ash aggregate-bearing part is usually diffuse; thickness ratio of the two parts defines two subtypes: i) equal thickness across most of the layer; ii) in the middle part of subunit B (layer 6,7,8 and 10), the upper part is eight to ten times thicker than the basal part; thickness of the coarser basal part often shows lateral variations at dm-scale, depending on small irregularities of the underlying microtopography; components: pumice fragments, abundant 1–2 mm-sized biotite, feldspar and amphibole phenocrysts and rare lithics; largest pumice fragments reach 3 cm in diameter, sometimes found at the base of an individual layer; small, cm-wide, vertical gas escape structures defined by the absence of fine ash and abundance of several mm-large pumice, lithic and phenocryst fragments and very diffuse low-angle cross-bedding in layer 12. *Ash aggregates*: 0.2–10 mm-sized ash aggregates with a relatively coarser core and a finer-grained rim and rim fragments are very abundant. *Granulometry*: basal part: Md ϕ: between 0.26 and 0.45; $\sigma\phi$: 1.61 and 1.93. Upper part: Md ϕ: between ~1 and 3.7; $\sigma\phi$: ~3; high $\sigma\phi$ values could be the consequence of the presence of cemented ash aggregate fragments, which did not decompose during soft crushing before grain-size analysis (c.f. Mueller et al., 2017). *Grain-size distribution*: basal part: symmetric normal peak at $\phi = 1$ (0.5 mm). Upper part: typical peak is centered at $\phi = 6$ (0.016 mm), in addition to the peak at $\phi = 1$, resulting in a bimodal grain-size distribution	All layers in subunit B	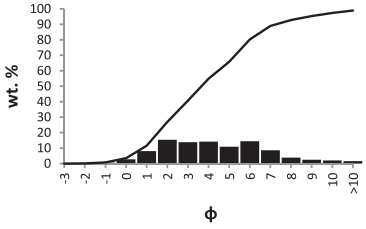	Deposit from dilute, wet pyroclastic density current
LF4	*Thickness*: 4–5 m (including the ~2 m thick altered zone at its top). *Lithology*: transitional lower contact with the underlying topmost layer of subunit B; diffuse bedding by slight grain-size variations; matrix-supported fine to coarse tuff; pumice clasts are supported in a fine-grained matrix; Ufacc ash aggregate fragments and 0.5–1 cm-sized pumice clasts are abundant in the lowermost 20 cm thick zone; meter-sized, irregular patches composed of 3–5 mm-sized pumice clasts, lithic clasts and phenocrysts free of fine ash showing clast-supported fabric, well-sorting at the lowermost 1.5 m thick zone; topmost ~2 m zone is heavily weathered, greenish brown zone with blocky microfabric. *Granulometry*: slight upward coarsening at Bogács (Md ϕ: 3 (1 m above its base), 1.7 (in the middle part), 1.2 (below the weathered zone); $\sigma\phi$: between 1.7 and 2.4). *Grain-size distribution*: two peaks at $\phi = 6$ (0.015 mm), and $\phi = 1$, resulting in a bimodal grain-size distribution	Subunit C	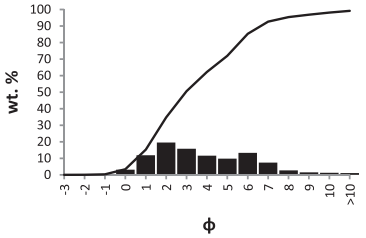	Phreatomagmatic ignimbrite

however, the degree of fragmentation of typical phreatomagmatic tephras is much higher than those found in dry magmatic ones (Self and Sparks, 1978; Cioni et al., 2015; Houghton et al., 2015a). The original spatial extent and total grain-size distribution of ancient successions displaying poor preservation are typically unknown. As a consequence, demonstration of the involvement of external water in ancient volcanic eruptions is usually challenging, and must be based either on the recognized characteristics of pyroclast textures, or on sedimentological features of the pyroclastic beds which can record (i) water influence on fragmentation at vent, (ii) presence of water in the eruption column, and also (iii) in the deposited tephra (Houghton et al., 2015b).

Once the following criteria (a-e) are determined, they can be used as proxies to identify the phreatomagmatic origin even for poorly exposed, ancient pyroclastic successions (cf. Houghton et al., 2015b): a) the

Fig. 6. Photographs showing subunits of the Jató Member and the internal structure of subunit A. A – The Jató Member at Bogács; B – The Jató Member at Tibolddaróc; C – The upper part of subunit C and its sharp upper contact with Unit III at Bogács; D – Subunit A and the lowermost part of subunit B at Bogács; E – Subunit A at Tibolddaróc. Note the bedded internal structure of subunit A, the constant thickness of the layers and the identical thicknesses at Bogács and Tibolddaróc.

amount of fine ash (sensu *lato*) is anomalously high (McPhie, 1986); b) ash aggregates are abundant and pumice clasts are often coated by a fine ash rim (coated pumice; Wilson, 2001; Ellis and Branney, 2010); c) PDC deposits are relatively fine-grained, non-welded and may contain uncharred plant detritus indicative of relatively low temperature (Porreca et al., 2008); d) the ash fraction is dominated by angular, blocky ash particles (Scarpati et al., 1993; Ellis and Branney, 2010; Shoji et al., 2018), characterized by solidity (area of the particle/area of the convex hull) and convexity (perimeter of the convex hull/perimeter of the particle) values dominantly between 0.8 and 1.0, i.e. higher (Liu et al., 2015) than for ash from dry magmatic eruptions (Heiken and Wohletz, 1985); e) presence of diatoms (algae skeletons) in the volcanic ash as a result of incorporation of surface water into the ejecta (Van Eaton et al., 2013; Houghton et al., 2015b).

None of the above features alone is exclusive fingerprint of a phreatomagmatic origin, and the discrimination between magmatic and phreatomagmatic tephra origin is difficult and often subjective, as addressed recently for many volcanic eruption styles (White and Valentine, 2016). For instance, the presence of ash aggregates is not necessarily a sign that magma fragmentation was driven by molten fuel-coolant interactions (MFCI) between magma and water; the presence of condensed water available in the eruption clouds may also lead to the same result (Brown et al., 2010; Palladino and Taddeucci, 1998; White and Valentine, 2016). Ash aggregates can be formed within the eruption cloud charged with fine ash encountering a moist atmospheric region (e.g. a cloud) or because of the presence of large amounts of steam gradually condensing from the eruption cloud itself and rising to higher atmospheric levels (Folch et al., 2010; Houghton et al., 2015a). Moreover, unusually high fragmentation values were also observed in pyroclastic successions derived from magmatic eruptions such as those from the third phase of the Eyjafjallajökull 2010 eruption (Dellino et al., 2012).

Despite all the above listed uncertainties, presence of fine-rich and ash aggregate-bearing pyroclastic units deposited between coarser grained ash aggregate-free layers are considered to be good indicators

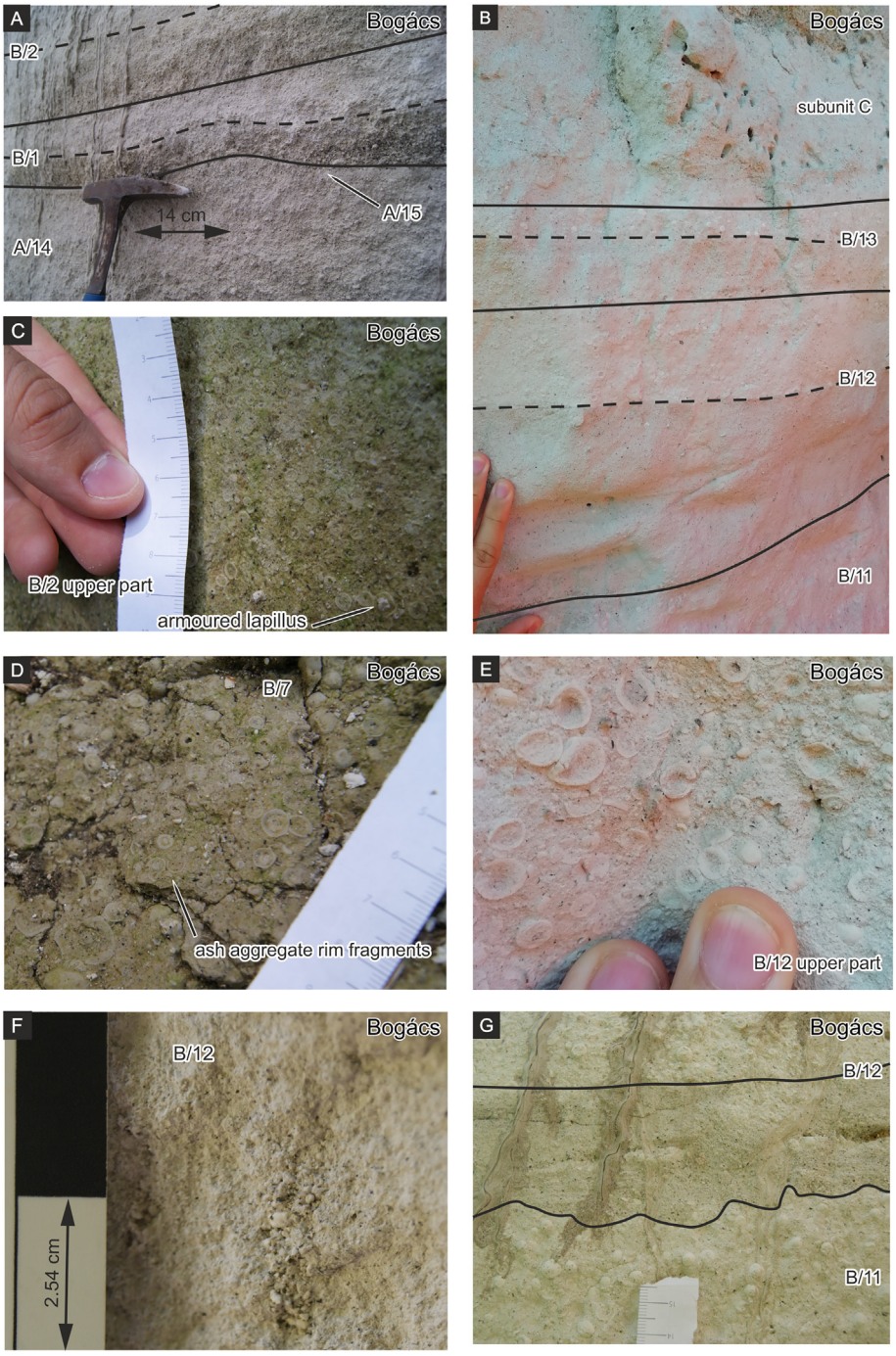

Fig. 7. Appearance of LF3 in subunit B at Bogács. A – Typical internal structure of LF3 in subunit B – coarse-grained lower part and fine-grained upper part with high amount of ash aggregates. Dashed line separates the coarse-grained lower part and fine-grained upper part in each picture. B – The contact between subunit B and C. Note the thickness difference in layer B/12 compared to picture G. C – Ash aggregates showing normal grading in the upper part of layer B/2. Scale units in centimeters. D – Layered ash aggregates in layer B/7; Note the abundant ash aggregate rim fragments. E – Upper part of layer B/12 full of layered ash aggregates with fine-grained rim and fragments. F – Small gas escape structure in layer B/12. G – The boundary between layer B/11 and B/12. Note the abundance of ash aggregates at the top of B/11 and the faint fine bedding of B/12. Scale units in centimeters.

of pulsating water influence in ancient, poorly constrained successions, emplaced from the same source in a short period of time. Some of them are composed of layers originating from alternating dry magmatic and phreatomagmatic phases (McPhie, 1986; Branney, 1991; Wilson, 2001; Ellis and Branney, 2010). If groundwater or surface water is available in the vent location, the suddenly heated water can provide large volumes of steam to the eruption cloud and, consequently magma fragmentation at the vent would likely be driven or at least heavily enhanced by the presence of water. Such a model has been applied for major silicic Phreatoplinian eruptions such as the 25.4 ka Oruanui, the AD 183 Taupo eruptions, and many other ignimbrite-forming eruptions in the central part of the North Island of New Zealand during the last 1.5 million years (Wilson and Walker, 1985a, 1985b; Wilson, 1993; Wilson, 2001; Manville and Wilson, 2004; Wilson et al., 2006; Van Eaton et al., 2013), the ~70 ka Neapolitan Yellow Tuff from the Campi Flegrei caldera in Italy (Cole and Scarpati, 1993), the 161 ka Kos Plateau Tuff from the Eastern Aegean (Allen and Cas, 1998), and the Askja AD 1875 layer C (Sparks et al., 1981).

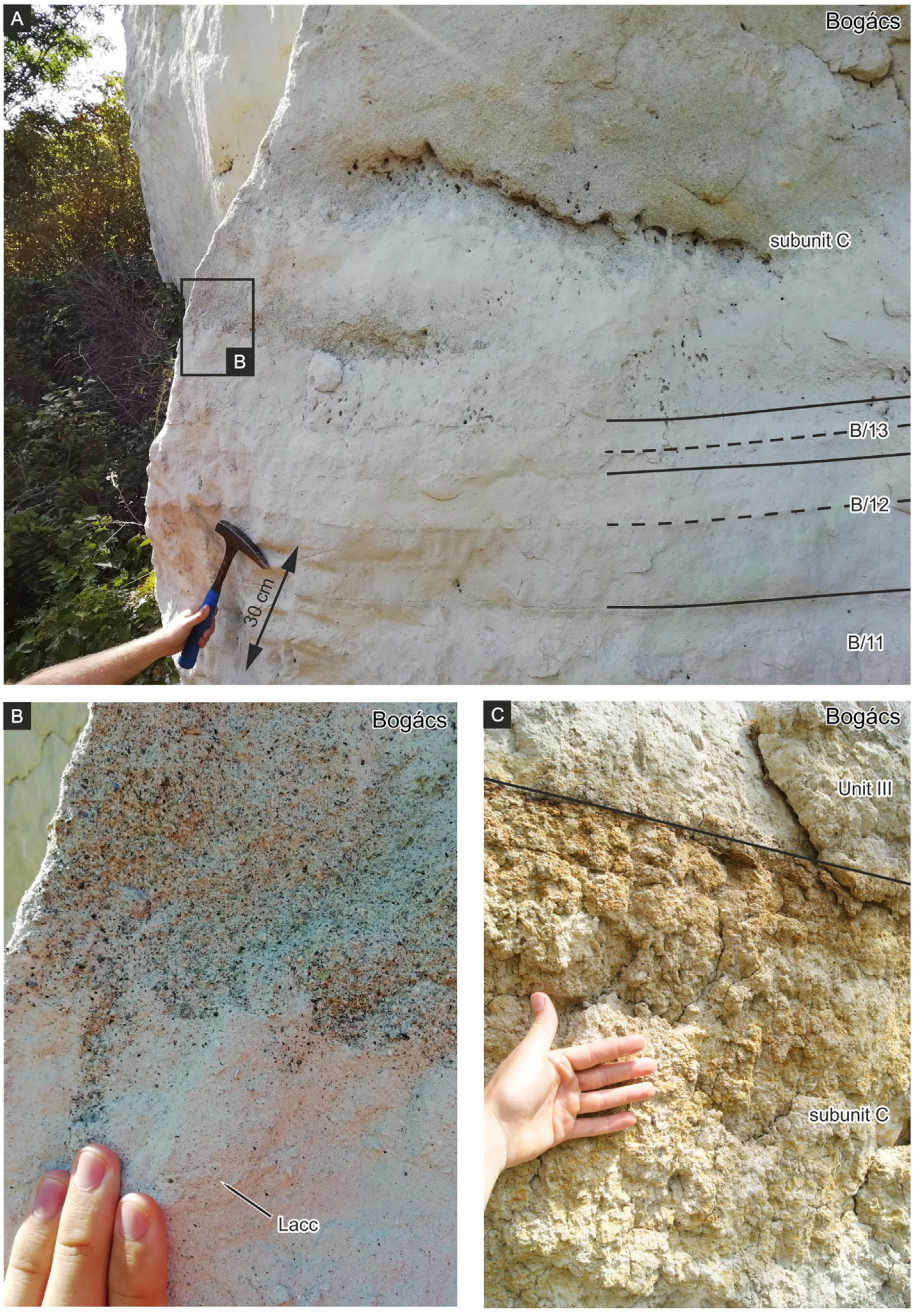

Fig. 8. Features of subunit C at Bogács. A – Contact between subunit B and C. Hammer length is 30 cm. B – Close-up view of the irregular, grain supported zone. Location of the close-up photographs is marked on picture A. Lacc marks a layered ash aggregate.; C – The uppermost, weathered zone of subunit C.

5.2.2. Transformation from dry fallout- to wet PDC-dominated deposition

The constant thickness, the unimodal grain-size distribution (Table 2.; Lirer et al., 1973; Scasso et al., 1994; Wilson, 2001) and the well-sorted character of LF1, which is the main constituent of subunit A, imply a pyroclastic-fall origin (cf. Walker and Croasdale, 1971; Walker, 1971). Thus, subunit A records the initial fallout-dominated phase of a Plinian eruption. The presence of LF2 indicates episodically increasing fragmentation. Alternating relatively coarse-grained (i.e. LF1) and fine-grained (LF2) layers in stratified Plinian sequences are common, mainly attributed to intermittent collapse of the eruption column (Walker, 1981b; Fierstein and Hildreth, 1992; Talbot et al., 1994; Palladino and Taddeucci, 1998), or to the episodic transition from dry magmatic to phreatomagmatic activity for short periods of time during an ongoing eruption (Scasso et al., 1994).

The AMS data from layer 13 supports to interpret LF2 as PDC deposit. Most of the PDC deposits show directional fabric due to the presence of shearing in the depositional regime just before the emplacement (Branney and Kokelaar, 2002; Ort et al., 2015). AMS studies of various PDC deposits pointed out, that directional fabric develops in base surge deposits (Cagnoli and Tarling, 1997), low volume confined and large volume unconfined ignimbrites (Porreca et al., 2003, Ort et al., 2003, Dedzo et al., 2011). Hence, well-clustered principal susceptibilities as a result of preferred-orientation of magnetic particles according to a directional fabric is considered as a general feature of PDC deposits (Cañón-Tapia and Mendoza-Borunda, 2014). From the layers analysed by AMS only layer 13 from subunit A is characterized by a preferred grain orientation, revealed by P′ values of ~0.5–1.2% and good clustering of principal susceptibilies (Figs. 5, 9). Such P′ values are lower, than the

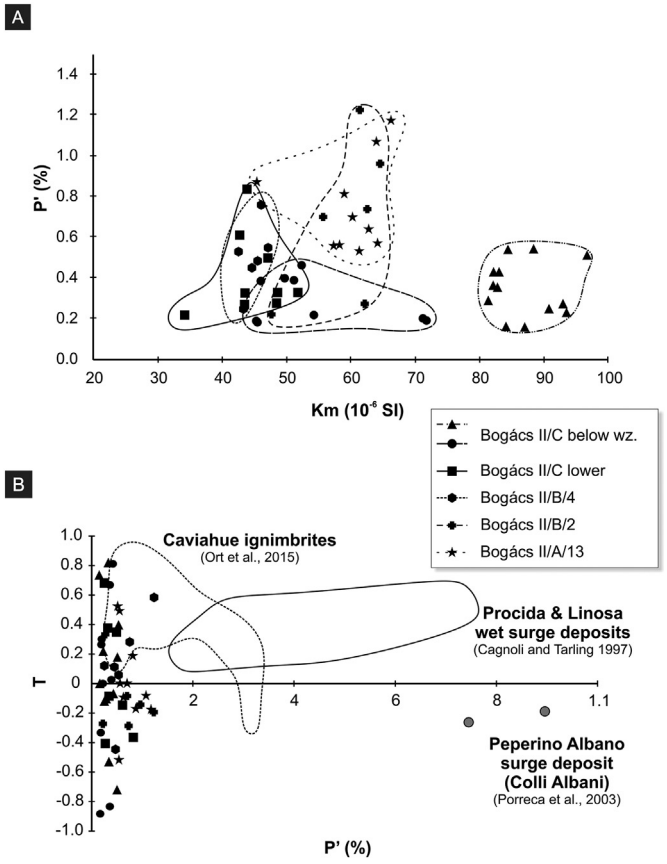

Fig. 9. Shape anisotropy of magnetic susceptibility ellipsoids from the Jató Member. For location of samples and stereographic projections see Fig. 5. a) Corrected degree of anisotropy (P′) vs. mean magnetic susceptibility (Km). Note, that P′ is independent from Km. b) Shape parameter (T) vs. corrected degree of anisotropy (P′) of investigated samples and various reference pyroclastic density current deposits.

typical values (>2%) obtained from base surge deposits and typical ignimbrites with directional fabric (Cagnoli and Tarling, 1997, Dedzo et al., 2011, Ort et al., 2003). The observed vertical clustering of K_{min} and good clustering of K_{max} in an E-W subhorizontal direction is identical to the "lineated and foliated" type AMS facies, which is formed, when emplacement of pyroclastic material occurs from a basal depositional system of a density-stratified current characterized by high particle concentration compared to the overriding current (Ort et al., 2015). Alternatively, such well-clustering of principal susceptibilities was observed from eolian sediments and fluvial resedimented materials (Tarling and Hrouda, 1993). However, in our case, deposition under heavy wind conditions or redeposition by wind is not supported by the obtained grain-size distribution showing only moderate sorting (the σφ values as an indicator of sorting are higher than 2 from most LF2 layers). Moreover, layer 13, which was sampled for AMS analysis shows identical thickness of 25 cm both at Bogács and Tibolddaróc, and is free of signs of eolian reworking, i.e. cross-bedding and depletion of fines (Smith and Katzman, 1991) or fluvial resedimentation, i.e. cross-stratification, laminated structure (Kataoka and Nakajo, 2002; Kataoka, 2003; Manville and Wilson, 2004).

Subunit B records a significant change in eruption style characterized by multiple wet PDC pulses. Its PDC origin supported by the type and distribution of ash aggregates within individual layers (Table 2). Relatively larger layered ash aggregates (0.5–1 cm in diameter) with a distinctively finer-grained outer rim, are distributed sparsely in the middle part of LF3 layers. Towards the upper boundary of individual layers, such layered ash aggregates with a finer outer rim become more abundant and typically smaller (2–5 mm in diameter). A systematic study on the internal structure and distribution of ash aggregates found in deposits from pyroclastic flows and surges and co-ignimbrite as well as co-surge ash clouds at the Laacher See volcano showed a clear relationship between the emplacement mode of a layer and the features of ash aggregates (Schumacher and Schmincke, 1991). Namely, "Rim-type lapilli" consisting of a coarser-grained core and an outer fine-grained rim were observed at the upper part of individual, thin PDC deposits. Besides the PDC deposits of the Laacher See volcano, the observed distribution of ash aggregates was described in the wet surge deposits of the 1982 eruption of El Chichón in Mexico (Scolamacchia et al., 2005), the thin PDC deposits of the Poris Formation at Tenerife (Brown et al., 2010) and from the normal-graded, several cm-dm thick PDC members of the 25.4 ka Oruanui eruption in New Zealand (Van Eaton and Wilson, 2013). Such beds are interpreted to be emplaced from low density, turbulent, dilute PDCs (resulting in the lower, relatively coarser-grained part), followed by fallout of ash aggregates from an overlying wet co-PDC ash cloud (Scolamacchia et al., 2005; Brown et al., 2010). Layered ash aggregates with a finer outer rim of the 25.4 ka Oruanui ignimbrites were originated from a hybrid cloud system with a spreading stratified column and a co-ignimbrite ash domain (Wilson, 2001; Scolamacchia et al., 2005; Van Eaton and Wilson, 2013). In this process, ash pellets formed in the vent-derived plume and reentrained into the co-PDC ash clouds, where the outer, distinctively finer-grained rim developed (Houghton et al., 2015b). Abundant ash aggregate fragments in layers of subunit B imply abrasion and/or dismembering of ash aggregates during lateral transport within PDCs, as it was observed from several cm-dm thick phreatomagmatic PDC deposits of the 25.4 ka Oruanui eruption (Van Eaton and Wilson, 2013; Houghton et al., 2015b). The presence of several cm-sized gas escape structures – a common feature of laterally emplaced pyroclastic currents – (Fig. 7f) in layer 12 is also consistent with a PDC origin.

In addition, the AMS measurement revealed isotropic magnetic fabric with P′ values generally lower than 0.5% and isotropic distribution of principal susceptibilities from the middle or upper part of LF3 layers (Figs. 5 and 9). Base surge deposits and medial to distal ignimbrites are usually characterized by P′ values between 2 and 10% (Cagnoli and Tarling, 1997; Ort et al., 2003) and well-clustered principal susceptibilities occur as a result of flow-parallel alignment of particles or imbrication in the depositional regime (Branney and Kokelaar, 2002; Ort et al., 2015). Consequently, the following clustering of principal susceptibilities were observed: i) well-clustered vertical K_{min} axes, well clustered, K_{max} axes on the horizontal plane pointing towards the flow direction; ii) well-clustered K_{min} axes tilted away from vertical, K_{max} and K_{int} axes intermixing on a gently dipping foliation plane (see Fig. 10 in Giordano et al., 2008 for further description). The emplacement of LF3 layers from low density, turbulent, dilute PDCs an overlying wet co-PDC ash cloud is further supported by the absence of such magnetic fabric. As a conclusion, based on these observations, we infer that subunit B was built up from multiple, dilute and wet PDC pulses. There is a transitional contact between subunit B and the diffusely bedded tuff of subunit C, which also contains the same layered ash aggregates and fragments at its base. Gas escape structures are also observed in subunit C (Fig. 8a, b), implying its PDC origin. In addition, Mdϕ and σϕ values of subunit C (specified as LF4) overlap with those of the ignimbrite of the Kos Plateau Tuff (Unit B; Allen and Cas, 1998) and the fine-grained ignimbrites of the 25.4 ka Oruanui eruption (Fig. 10. Self, 1983; Wilson, 2001). Thus, we infer the tuff of subunit C to be the final ignimbrite of the succession, emplaced from density currents generated by the collapse of the eruption column (Branney and Kokelaar, 2002). It is not possible to decide whether subunit C was water-rich compared to the wet PDCs of subunit B. It lacks ash aggregates at its upper part, which allows the following eruption scenarios: i) The closing phase of the eruptional phase that produced the ignimbrite of subunit C was dry, because the external water was used up in the former phases, especially, which produced subunit B and subunit C emplaced from a relatively

dry closing PDC blast. ii) Based on its fine grain-size similar to many ignimbrites of the 25.4 ka Oruanui eruption (Fig. 10, Wilson, 2001) it could be produced also by a wet PDC-generating eruption. In this case, the upper co-ignimbrite ash containing abundant ash aggregates as an indicator of the water-rich nature of the ash cloud was eroded/altered by heavy weathering. The AMS properties of subunit C are identical to LF3 (Figs. 5, 9). According to the discussion above on the lack of PDC-related magnetic fabric in subunit C, it is also suggested to be deposited from low density currents, without density stratification resulted in a basal depositional layer characterized by lateral traction (Branney and Kokelaar, 2002; Ort et al., 2015). Alternatively, low P′ values can be attributed to very low mean susceptibilities, i.e. the scarcity of ferromagnetic particles in the samples (Rochette, 1987; Hrouda and Jelinek, 1990). Mean magnetic susceptibility of the Procida, Linosa, Pepperino Albano pyroclastic surge deposits and the Caviahue ignimbrite is between 800 and 5000 $\times 10^{-6}$ SI (Cagnoli and Tarling, 1997; Porreca et al., 2003; Ort et al., 2015). Hence, it is possible, that the existing fabric could not be revealed by AMS technique.

The abrupt change in the depositional regime from a fallout dominated into a collapsing column with the appearance of ash aggregates records a sudden enhancement of water vapour in the eruption column. There are no directly observable signs of erosion or weathering within the Jató Member. This, along with the identical phenocryst assemblage of feldspar, biotite and amphibole of the entire succession implies that the member was aggraded from one single eruption event in a short period of time, possibly within hours to months. The initially sustained eruption transformed into a periodically and then fully collapsing column may have resulted in the emplacement of subunit B and C due to the increased water-magma interaction at the vent (Fig. 11). Numerical experiments on column stability at a constant magma eruption rate and changing surface water content (0–40% by mass) indicated a pulsating eruption column and ascent of pyroclastic material from PDCs (i.e. dilute PDC pulses spreading outwards from the vent zone) when a significant quantity of external water was available (Van Eaton et al., 2012). The 232 AD Taupo and the 25.4 ka Oruanui eruption in New Zealand are good analogues; in these cases, the interaction of silicic magma with a caldera lake resulted in sustained eruptions with temporarily changing water influence producing successions of fallout and PDC deposits (Wilson, 2001, 1985, Van Eaton et al., 2012). It was documented, that ash aggregates could appear in pyroclastic successions due to entrainment of atmospheric water into the eruptional column during pyroclast dispersal in the atmosphere (Gilbert and Lane, 1994; Houghton et al., 2015a; White and Valentine, 2016). For example, ash aggregates fell during the eruption of the Sakurajima on 22 May in 1983 under humid weather (Gilbert and Lane, 1994), even if, these ash aggregates lacked the outer relatively fine-grained layers (Gilbert and Lane, 1994), thus were different from the ones observed in subunit B and C of the Jató Member. The entrainment of atmospheric water vapour in large silicic eruptions is generally limited (Glaze and Baloga, 1996), but sometimes the eruption column is able to incorporate a high amount of atmospheric moisture due to the interaction with water-rich typhoon clouds, as it happened during the 15 June 1991 climactic phase of the Pinatubo eruption (Houghton et al., 2015a). As a consequence, rain-flushing of fine ash and mud rain resulting in water-saturated tephra layers were observed. Nevertheless, it is important to note that fine-grained and layered PDC deposits from the Pinatubo eruption are free from ash aggregates and any signs of wet deposition are absent (Scott et al., 1996). Hence, the presence of ash aggregates in the Jató Member is more probably the result of phreatomagmatism.

5.2.3. Silicic phreatomagmatism at a subsiding back-arc basin setting

The influence of external water on the eruption style progressively increased with time successively in the Jató Member. Gradual enlargement of the vent area (e.g. gradual caldera subsidence) could result in a time-progressive increase of water-influence simply by letting the available surface water access to the vent via a foundering caldera. Similar increasing water-influence during the eruption was described from the Minoan Tuff (Bond and Sparks, 1976). The first phase of the Minoan eruption produced plinian pumice fall, but the second and third phases were phreatomagmatic due to vent migration to the partly flooded ancient caldera (Heiken and McCoy, 1984; Druitt et al., 1989, 1999, 2019; Druitt, 2014). A similar scenario is proposed for the formation of the 7.6 Ma old Akdag-Zelve ignimbrite in the Central or Cappadocian Volcanic Province (Central Anatolia; Schumacher and Mues-Schumacher, 1997). Possibly, at the BFVA, the initial dry eruptions which resulted in the aggradation of subunit A weakened the vent wall, which allowed the infiltration of sea or lake water into the vent to produce the phreatomagmatic layers of subunit B and C.

As mentioned in Section 2, the Early-Middle Miocene silicic intrabasinal volcanism of the CPR lasted for as long as 10 My (Pécskay et al., 1995, 2006). This time interval was also the time of most intense back-arc subsidence (Balázs et al., 2016), which resulted in multiple transgressions of the Central Paratethys and a continuous sea coverage in the CPR (Kováč et al., 2017). Therefore, water influence could have been a general feature of the Miocene silicic volcanism of this region.

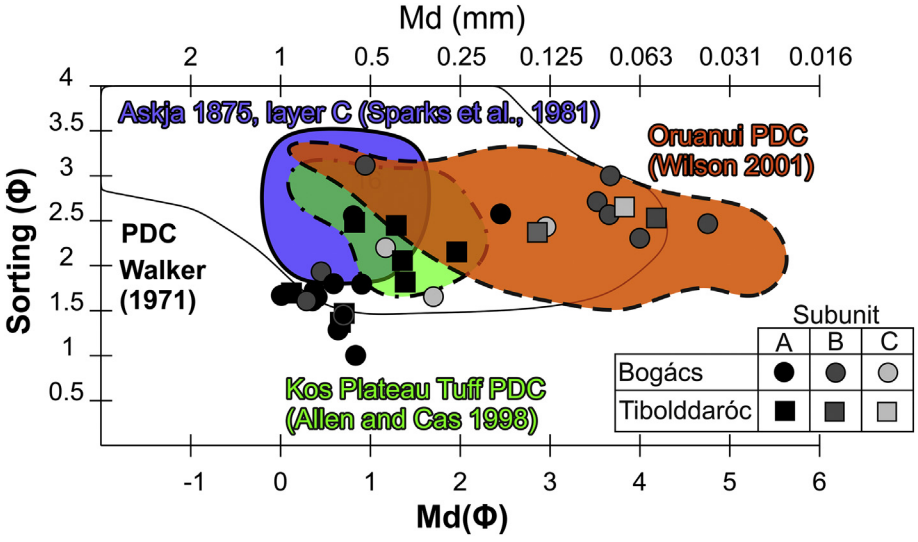

Fig. 10. Comparison of median grain size (Mdϕ) and sorting ($\sigma\phi$) of the Jató Member with fine-grained pyroclastic density current deposits published previously from Phreatoplinian successions.

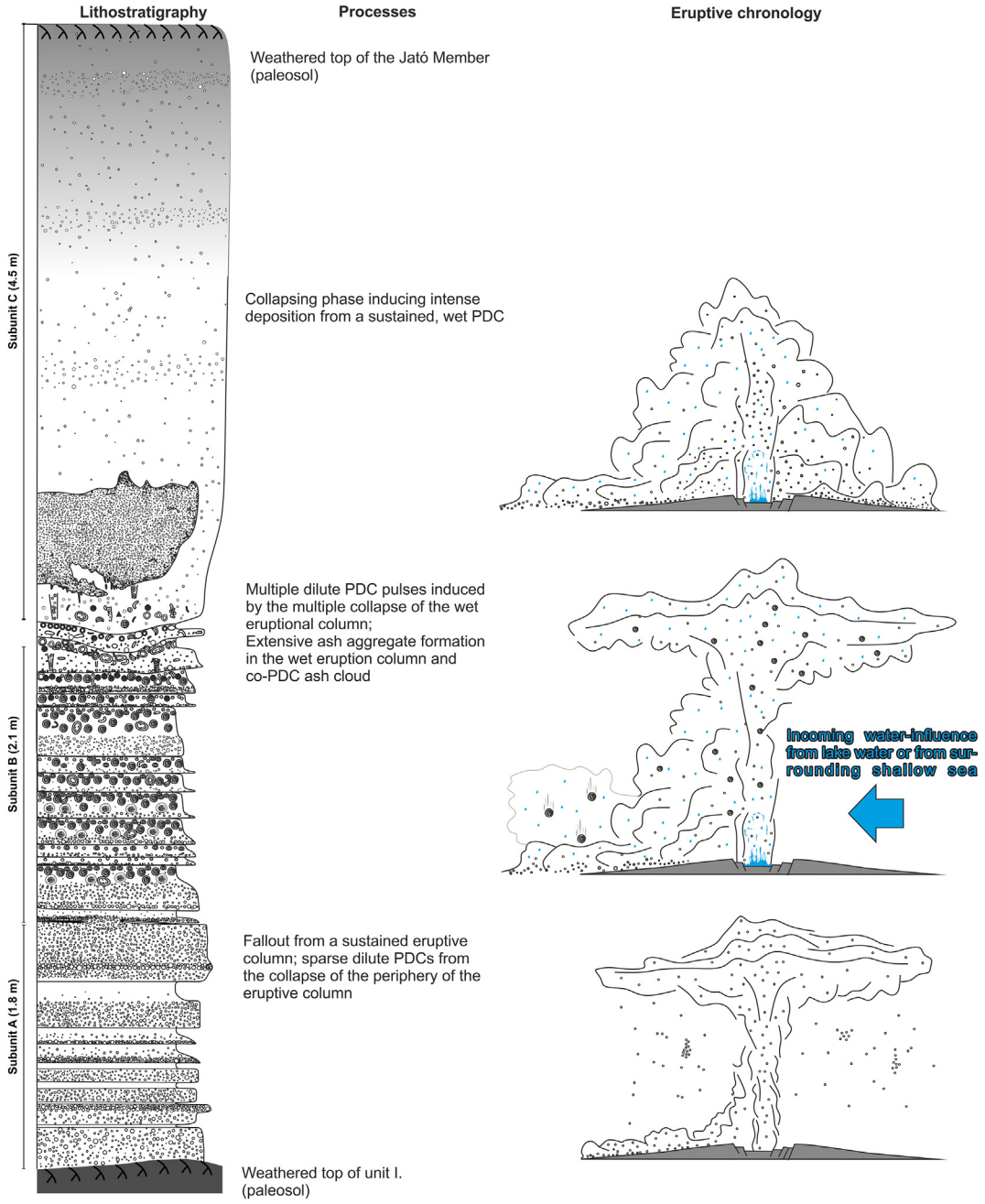

Fig. 11. Interpreted eruption and depositional processes (right) resulted in the generation of the Jató Member (left). Symbols of the lithological column are the same as in Fig. 5.

The availability of surface or shallow subsurface water in a large quantity in Middle Miocene times at the northern part of the Pannonian Basin is also supported by paleogeographical and paleoenvironmental reconstructions. The interpreted eruption age of an ash-flow tuff in the Tibolddaróc Succession, which belongs to the Demjén ignimbrite chrono- and chemostratigraphical unit, considered to be identical with subunit C of the Jató Member, is 14.88 ± 0.014 Ma (Lukács et al., 2018). Thus, the deposition of the hydromagmatic succession occurred in the Lower Badenian stage in the Central Paratethys chronostratigraphy (Kováč et al., 2007) corresponding to the end of the Langhian stage in the standard chronostratigraphic chart (Piller et al., 2007). At that time, large parts of the intrabasinal CPR subsided in a NE-SW extensional setting (Horváth et al., 1986), which led to the formation of numerous half-grabens (Balázs et al., 2016). The incrementally subsiding area was occupied by an arm of the Central Paratethys, which was an inland sea of the CPR, with connection to the broader Tethys and the global ocean (Kováč et al., 2007). Extension-driven subsidence along with global sea level rise resulted in stepwise transgression of the Central Paratethys from SE to NE during the Badenian in three phases: 16.3–16.2 Ma, ~14.7 Ma and 13.6–13.4 Ma (Kováč et al., 2007). Consequently, the intrabasinal part of the CPR was reconstructed as an archipelago, with several 10^2–10^3 km^2 large land patches (Kováč et al., 2007, 2017) and much larger areas covered by shallow to deep sea. The Bükk Mts. and their surroundings including the BFVA might have been subaerial terrains (Fig. 12; Bérczi et al., 1988; Szakács et al., 1998; Kováč et al., 2017). This reconstruction is also supported by the presence of paleosols in the succession between Bogács and Harsány Ignimbrites. The exact location of the source vents which produced the BFVA pyroclastic succession is unknown. Directional magnetic fabric of ignimbrites, areal extent of welding, pyroclast transport direction indicators (Szakács et al., 1998), lateral facies variations (Lukács et al., 2015), relative thickness, and a great number of thick ignimbrites

found in boreholes east of BFVA (Lukács et al., 2010), imply that the source vent(s) must have been somewhere along a belt in the northernmost part of the Great Hungarian Plain southward direction of BFVA (Fig. 12). This area corresponds to the northern part of the Jászság basin (Fig. 12), and comprised rapidly subsiding areas hosting shallow marine depocenters from the Early to Late Miocene (Kováč et al., 2007; Balázs et al., 2016). Thus, the location of vents in a shallow sea or at marshy lowland setting is likely to have existed in relation to the second Middle Miocene transgression of the Central Paratethys suggested at around ~14.7 Ma (Kováč et al., 2007), i.e. at the same time when the Jató Member was emplaced.

6. Conclusions

A new occurrence of pyroclastic deposits from the Miocene Bükk Foreland Volcanic Area (BFVA) in Northern Hungary, called the Jató Member is presented here in detail. The ~8 m thick layered pyroclastic succession was deposited in the Middle Miocene, ~14.9 Ma ago (Lukács et al., 2018) and was produced by silicic phreatomagmatism. Eruption processes were reconstructed on the basis of two well-preserved occurrences ~8 km apart, deposited ca. 10–50 km from the eruption center and offering an opportunity to perform detailed field and granulometrical analyses in spite of the old age of the succession. Heavily weathered pyroclastic material interpreted as paleosols were found below and at the top of the Jató Member implying quiescence periods before and after the explosive eruption. Weathered zones or erosional surfaces/redeposited material is not presented within the Jató Member, which, along with a homogenous phenocrystal assemblage of feldspar, biotite and amphibole, indicate deposition in a single eruption phase of hours to months.

Three subunits (A to C) were discriminated in the Jató Member: subunit A, 1.8 m thick, a series of fine ash to lapilli tuff layers with laterally constant thickness at an outcrop scale and unimodal grain-size distribution; 2) subunit B, 2.1 m thick, a series of normal-graded layers with an upper fine-grained zone containing abundant – in some layers exclusive – ash aggregates with a coarser core and fine outer rim; 3) subunit C, 4.5 m thick, a massive, poorly to well-sorted coarse ash with gas escape structures and ash aggregates at its base. The successive change of the recorded lithofacies from base to top of the section implies an initially dry fallout-dominated deposition of ash (subunit A) transforming into a wet regime emplaced by multiple pyroclastic density current pulses (subunit B and C). The general abundance of PDC-related ash aggregates in the middle-upper part of the succession, and the transformation of a fall-dominated to a collapsing depositional regime producing wet ignimbrites imply increasing water influence on a silicic eruption (Phreatoplinian sensu *lato*). Because the formation of the Jató Member

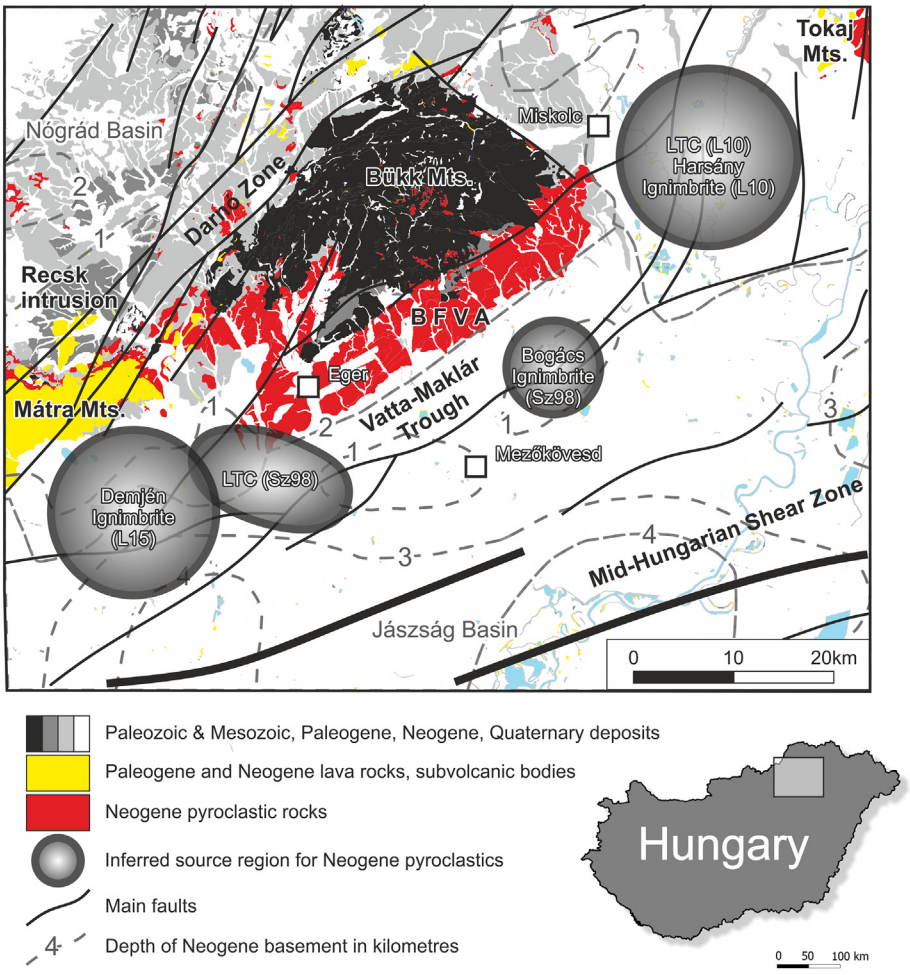

Fig. 12. Inferred volcanic source regions for various pyroclastic deposits of the BFVA (Sz98 – Szakács et al., 1998; L10 – Lukács et al., 2010; L15 – Lukács et al., 2015) in relation with structural units and zones of Neogene-Quaternary subsidence. LTC is Lower Tuff Complex including the Eger and Mangó Ignimbrites. Basemap: surficial geological map of Hungary published by the Mining and Geological Survey of Hungary (https://map.mbfsz.gov.hu/fdt100/). Fault lines were adopted from Beke et al. (2019) and the Neogene basement isolines from Horváth and Royden (1981).

was coeval with extensive seawater cover due to regional basin subsidence, the source of external water at the site of eruption suggested to have been in the form of a caldera lake or shallow sea around a volcano.

The obtained results have the following general implications:

i) Eruption scenario of successions from silicic explosive volcanism even as old as ~15 Ma could be established if one or more outcrops allow investigating the entire succession layer by layer.
ii) Recognizing the transition from dry magmatic fallout activity to emplacement of wet PDCs producing layers rich in ash aggregates is an effective way to reveal increasing phreatomagmatic (sensu lato) character. Such a successive change is typical when external water gets into contact with the eruption after an initial dry phase due to opening of the crater wall and infiltration of the surrounding lake or sea water.
iii) Silicic phreatomagmatism may have been typical in the Carpathian-Pannonian region during Miocene times. Thus, the Bükk Foreland Volcanic Area in North Hungary and the neighbouring ignimbrite fields could offer an opportunity to study ancient Phreatoplinian successions.

CRediT authorship contribution statement

Tamás Biró: Conceptualization, Methodology, Investigation, Writing - original draft.**Mátyás Hencz:**Conceptualization, Methodology, Investigation, Writing - original draft.**Károly Németh:**Conceptualization, Investigation, Writing - original draft.**Dávid Karátson:**Conceptualization, Investigation, Writing - original draft.**Emő Márton:**Methodology, Investigation.**Alexandru Szakács:**Conceptualization, Investigation.**Balázs Bradák:**Methodology, Formal analysis.**Zoltán Szalai:**Methodology, Investigation.**Zoltán Pécskay:**Conceptualization.**István János Kovács:** Conceptualization.

Acknowledgments

Physical volcanological research of TB is supported by ÚNKP-16-3 New National Excellence Program of the Ministry of Human Capacities and the National Talent Program – Young Talents of the Nation (NTP-NFTÖ-18-B-0130). This work was supported by the Hungarian Scientific Research Fund project nos. K105245, K115472, K128625, K131894, K128122 and by the European Union and the State of Hungary, co-financed by the European Regional Development Fund in the project of GINOP - 2.3.2 - 15 - 2016 - 00009 ICER. KN's contribution and field work were possible by the fund available under the Erasmus+ International Credit Mobility, - ELTE – Massey University Research Cooperation Program. Balázs Bradák acknowledges the financial support of project BU235P18 (Junta de Castilla y León, Spain) and the European Regional Development Fund (ERD). Zoltán Cseri (Eötvös University, Department of Physical Geography) is greatly acknowledged for conducting AMS measurements, whereas Katalin Fehér (Eötvös University, Department of Environmental and Landscape Geography) for her help during sieving and density measurements. We thank Annamária Nagy (Research Center for Astronomy and Earth Sciences, Geographical Institute) for her assistance in laser diffraction measurements. Comments and language editing by Julie Palmer are highly appreciated. Comments and suggestions from Alexa Van Eaton (U.S. Geological Survey) and Geoff Kilgour (GNS Science, New Zealand) that enriched the original version of the manuscript are greatly acknowledged. Thanks go to José Luis Macías for useful comments and editorial handling of the manuscript.

Declaration of competing interest

The authors declare that they have no known competing financial interests or personal relationships that could have appeared to influence the work reported in this paper.

Appendix A. Materials and methods

A.1. Granulometry

Disaggregation of samples was performed carefully by bare hand or applying wide, soft rubber bands to avoid artificial crushing of pumices and glass shards. The samples were dried before granulometric analysis in an oven at 105 °C for at least 1.5 h. The analyses were conducted in two steps: i) fractions coarser than 0.063 mm were sieved for ~20 min; ii) fractions finer than 0.063 mm were analysed by laser diffractometry. 100-1300 g per sample (<500 g from fine tuffs and >500 g from coarse tuffs and lapilli tuffs) were sieved. Sieves with 8, 4, 2, 1, 0.5, 0.25, 0.125 and 0.063 mm mesh size were used. Grain-size distributions from sieving were expressed in one ϕ-sized classes:

$$\phi = -\log_2 d \tag{A.1}$$

where, d is grain diameter. Laser diffraction measurements were performed in the Geographical Institute in the Research Center for Astronomy and Earth Sciences of Hungarian Academy of Sciences in Budapest by using a Fritsch Analyzette 22 MicroTec Plus instrument. Diameters of grains were determined by using the Mie theory and considering 1.54 refractive index and 0.1 extinction coefficient. Three measurements of each 0.3-0.5 g sample were performed after ultrasonic treatment. The three grain-size distributions were identical in all cases. Grain-size distributions resulted from laser diffractometry were merged into ϕ classes within the range of 5 to 10 ϕ (i.e. from 0.031 to 0.001 mm). Grain-size distributions obtained from sieving are expressed in weight percentages. On the contrary, laser diffraction results are expressed in volume distribution of the grain-size classes. If the density is homogeneous, the two distributions can be merged according to the simple formula:

$$\rho = \frac{m}{V} \tag{A.2}$$

where, ρ is the density, m is the mass and V is the volume. Under binocular microscope all fractions finer than 0.063 mm contained >95% glass shards, thus considered to be homogeneous with respect to density. Bulk density of the <0.063 mm fraction was also checked by a pycnometer for several samples. The obtained densities range between 2.25 and 2.41 g/cm^3, that is, the typical density of a dense rhyolitic glass (Tilley, 1922), which also indicates the homogeneous density of the <0.063 mm fraction. Thus, data expressed in weight percent from sieving (from -3 to 4 ϕ) and from laser diffractometry (from 5 to 10 ϕ) were simply combined. Grain-size distributions were described by using the following parameters: median diameter (Mdϕ) and sorting ($\sigma\phi$) of Inman (1952) according to the following formulas:

$$\mathrm{Md}\phi = \phi 50 \tag{A.3}$$

$$\sigma\phi = \frac{\phi 84 - \phi 16}{2} \tag{A.4}$$

where Mdϕ is the median diameter and $\sigma\phi$ is the sorting expressed in ϕ. (ϕ50, ϕ84, ϕ16 are given grain-sizes below which the 50, 84 and 16% of the total population is finer.) The F2 value was also computed, which is the amount of the <1/16 mm (<0.063 mm) fraction, expressed in weight percent (Walker, 1983).

A.2. Anisotropy of magnetic susceptibility

Six to thirteen specimens from each site were measured. Porous samples were impregnated by Na_2SiO_3 in order to avoid disintegration during measurements. AMS measurements were performed at the Paleomagnetic Laboratory of the Mining and Geological Survey of Hungary in Budapest by using a KLY-2 Kappabridge instrument. AMS ellipsoid parameters were computed on the specimen level with a computer program (Bordás, 1990) based on Jelinek (1977), and on locality

level using Anisoft 4.2 (Chadima and Jelínek, 2008) based on Jelinek (1978). Parameters of the magnetic susceptibility ellipsoids were calculated according to Jelínek's statistical formulas (Jelinek, 1977, 1981). F-test was used to determine whether the magnetic fabric is significantly anisotropic:

$$F = 0.4\left(\tau_1^2 + \tau_2^2 + \tau_3^2 - X_b^2\right)/\sigma^2 \quad (A.5)$$

where F is the significance of F-test, $\tau_1 > \tau_2 > \tau_3$ are the eigenvalues, X_b is the bulk magnetic susceptibility and σ is the variance. Statistically significant anisotropy is evident if $F > 3.4817$. The shape of the susceptibility ellipsoids was described by the corrected degree of anisotropy (P′) and by the shape factor (T) according to the following formulas:

$$P\prime = \sqrt[2]{2\{(\eta_1 - \eta) + (\eta_2 - \eta) + (\eta_3 - \eta)\}} \quad (A.6)$$

$$T = \frac{2(\eta_2 - \eta_3)}{\eta_1 - \eta_3} - 1 \quad (A.7)$$

where $\eta_1 = \ln K_{max}$; $\eta_2 = \ln K_{int}$; $\eta_3 = \ln K_{min}$; $\eta = (\eta_1 + \eta_2 + \eta_3)/3$ in order.

Appendix B. Supplementary data

Supplementary data to this article can be found online at https://doi.org/10.1016/j.jvolgeores.2020.106973.

References

Allen, S.R., Cas, R.A.F., 1998. Rhyolitic fallout and pyroclastic density current deposits from a phreatoplinian eruption in the eastern Aegean Sea, Greece. J. Volcanol. Geotherm. Res. 86, 219–251.

Balázs, A., Matenco, L., Magyar, I., Horváth, F., Cloetingh, S.A.P.L., 2016. The link between tectonics and sedimentation in back-arc basins: New genetic constraints from the analysis of the Pannonian Basin. Tectonics 35, 1526–1559.

Beke, B., Fodor, L., Millar, L., Petrik, A., 2019. Deformation band formation as a function of progressive burial: Depth calibration and mechanism change in the Pannonian Basin (Hungary). Mar. Petroleum Geol. 105, 1–16.

Bérczi, I., Hámor, G., Jámbor, Á., Szentgyörgyi, K., 1988. Neogene sedimentation in Hungary. In: Royden, L.H., Horváth, F. (Eds.), The Pannonian Basin - A Study in Basin Evolution. vol. 45. AAPG Memoir, pp. 57–67.

Bond, A., Sparks, R.S.J., 1976. The Minoan eruption of Santorini, Greece. J. Geol. Soc. 132, 1–16.

Bordás, R., 1990. Aniso–Anisotropy Program Package for IBM PC. ELGI, Budapest.

Branney, M.J., 1991. Eruption and depositional facies of the Whorneyside Tuff: an exceptionally large-magnitude phreatoplinian eruption. Geol. Soc. Am. Bull. 203, 886–897.

Branney, M.J., Kokelaar, P., 2002. Pyroclastic density currents and the sedimentation of ignimbrites. Geol. Soc. Lond. Memoirs 27 (143 p).

Brown, R.J., Branney, M.J., Maher, C., Dávila-Harris, P., 2010. Origin of accretionary lapilli within ground-hugging density currents: evidence from pyroclastic couplets on Tenerife. Bull. Volcanol. 122, 305–320.

Büttner, R., Dellino, P., La Volpe, L., Lorenz, V., Zimanowski, B., 2002. Thermohydraulic explosions in phreatomagmatic eruptions as evidenced by the comparison between pyroclasts and products from Molten Fuel Coolant Interaction experiments. J. Geophys. Res. Solid Earth 107, B11. https://doi.org/10.1029/2001JB000511.

Cagnoli, B., Tarling, D.H., 1997. The reliability of anisotropy of magnetic susceptibility (AMS) data as flow direction indicators in friable base surge and ignimbrite deposits: Italian examples. J. Volcanol. Geotherm. Res. 75, 309–320.

Cañón-Tapia, E., Mendoza-Borunda, R., 2014. Magnetic petrofabric of igneous rocks: lessons from pyroclastic density current deposits and obsidians. J. Volcanol. Geotherm. Res. 289, 151–169.

Capaccioni, B., Corodannosi, N., Harangi, R., Harangi, Sz, Karátson, D., Sarocchi, D., Valentini, L., 1995. Early Miocene pyroclastic rocks of the Bükkalja Ignimbrite Field (North Hungary) - a preliminary stratigraphic report. Acta Vulcanol. 7, 119–124.

Chadima, M., Jelínek, V., 2008. Anisoft 4.2. – anisotropy data browser. Contrib. Geoph. Geod. 38, 38–41.

Cioni, R., Pistolesi, M., Rosi, M., 2015. Plinian and subplinian eruptions. In: Sigurdsson, H., Houghton, B., McNutt, S., Rymer, H., Stix, J. (Eds.), The Encyclopedia of Volcanoes, Second edition Academic Press, San Diego, pp. 519–535.

Cole, P.D., Scarpati, C., 1993. A facies interpretation of the eruption and emplacement mechanisms of the upper part of the Neapolitan Yellow Tuff, Campi Flegrei, southern Italy. Bull. Volcanol. 55, 311–326.

Csontos, L., Nagymarosy, A., Horváth, F., Kovác, M., 1992. Tertiary evolution of the Intra-Carpathian area: a model. Tectonophysics 208, 221–241.

Czuppon, Gy, Lukács, R., Harangi, Sz, Mason, P.R., Ntaflos, T., 2012. Mixing of crystal mushes and melts in the genesis of the Bogács Ignimbrite suite, northern Hungary: an integrated geochemical investigation of mineral phases and glasses. Lithos 148, 71–85.

Dedzo, M.G., Nédélec, A., Nono, A., Njanko, T., Font, E., Kamgang, P., Njonfang, E., Launeau, P., 2011. Magnetic fabrics of the Miocene ignimbrites from West-Cameroon: implications for pyroclastic flow source and sedimentation. Journal of Volcanology and Geothermal Research 203, 113–132.

Dellino, P., Gudmundsson, M.T., Larsen, G., Mele, D., Stevenson, J.A., Thordarson, T., Zimanowski, B., 2012. Ash from the Eyjafjallajökull eruption (Iceland): fragmentation processes and aerodynamic behavior. J. Geophys. Res. Solid Earth 117, B00C04.

Druitt, T.H., 2014. New insights into the initiation and venting of the Bronze Age eruption of Santorini, from component analysis. Bull. Volcanol. 76, 794.

Druitt, T.H., Mellors, R.A., Pyle, D.M., Sparks, R.S.J., 1989. Explosive volcanism on Santorini, Greece. Geol. Mag. 126, 95–126.

Druitt, T.H., Edwards, L., Mellors, R., Pyle, D.M., Sparks, R.S.J., Lanphere, M., Davies, M., Barriero, B., 1999. Santorini volcano. Geol. Soc. Lond. Mem. 19 (165 p).

Druitt, T.H., McCoy, F.W., Vougioukalakis, G.E., 2019. The late Bronze Age eruption of Santorini volcano and its impact on the ancient Mediterranean world. Elements 15, 185–190.

Ellis, B., Branney, J., 2010. Silicic phreatomagmatism in the Snake River Plain: the Deadeye Member. Bull. Volcanol. 72, 1241–1257.

Fierstein, J., Hildreth, W., 1992. The plinian eruptions of 1912 at Novarupta, Katmai national park, Alaska. Bull. Volcanol. 54, 646–684.

Folch, A., Costa, A., Durant, A., Macedonio, G., 2010. A model for wet aggregation of ash particles in volcanic plumes and clouds: 2. Model application. J. Geophys. Res. Solid Earth 115, B09202.

Gilbert, J.S., Lane, S.J., 1994. The origin of accretionary lapilli. Bull. Volcanol. 56, 398–411.

Giordano, G., Porreca, M., Musacchio, P., Mattei, M., 2008. The Holocene Secche di Lazzaro phreatomagmatic succession (Stromboli, Italy): evidence of pyroclastic density current origin deduced by facies analysis and AMS flow directions. Bull. Volcanol. 70, 1221–1236.

Glaze, L.S., Baloga, S.M., 1996. Sensitivity of buoyant plume heights to ambient atmospheric conditions: Implications for volcanic eruption columns. J. Geophys. Res. Solid Earth 1529–1540.

Gravley, D.M., Deering, C.D., Leonard, G.S., Rowland, J.V., 2016. Ignimbrite flare-ups and their drivers: a New Zealand perspective. Earth Sci. Rev. 162, 65–82.

Hámor, G., Ravasz-Baranyai, L., Balogh, K., Árva-Sós, E., 1979. K/Ar dating of miocene pyroclastic rocks in Hungary. Ann. Géol. Pays. Hellén Tome Horsserie 491–500.

Harangi, Sz, Lenkey, L., 2007. Genesis of the Neogene to Quaternary volcanism in the Carpathian-Pannonian region: role of subduction, extension, and mantle plume. Geol. Soc. Am. Spec. Pap. 418, 67.

Heiken, G., McCoy, F., 1984. Caldera development during the Minoan eruption, Thira, Cyclades, Greece. J. Geophys. Res. Solid Earth 89, 8441–8462.

Heiken, G.H., Wohletz, K., 1985. Volcanic Ash. University of California, Berkeley, p. 246.

Horváth, F., Royden, L., 1981. Mechanism for the formation of the intra-Carpathian basins: a review. Earth Evolution Science 1, 307–316.

Horváth, F., Dövényi, P., Laczó, I., 1986. Geothermal effect of magmatism and its contribution to the maturation of organic matter in sedimentary basins. In: Buntebarth, G., Stegena, L. (Eds.), Paleogeothermics, Lecture Notes in Earth Sci. vol. 5. Springer-Verlag, Berlin, Heidelberg, pp. 173–183.

Houghton, B.F., Wilson, C.J.N., Smith, R.T., Gilbert, J.S., 2015a. Phreatoplinian eruptions. In: Sigurdsson, H., Houghton, B., McNutt, S., Rymer, H., Stix, J. (Eds.), The Encyclopedia of Volcanoes, First edition Academic Press, San Diego, USA, pp. 513–525.

Houghton, B., White, J.D.L., Van Eaton, A.R., 2015b. Phreatomagmatic and related eruption styles. In: Sigurdsson, H., Houghton, B., Rymer, H., Stix, J., McNutt, S. (Eds.), The Encyclopedia of Volcanoes, pp. 537–552.

Hrouda, F., Jelinek, V., 1990. Resolution of ferromagnetic and paramagnetic anisotropies in rock, using combined low-field and high-field measurements. Geophys. J. Int. 103, 75–84.

Inman, D.L., 1952. Measures for describing the size distribution of sediments. J. Sedim. Petrol 22, 125–145.

Jelinek, V., 1977. The Statistical Theory of Measuring Anisotropy of Magnetic Susceptibility of Rocks and Its Application. Geofyzika Brno, Brno.

Jelinek, V., 1978. Statistical processing of anisotropy of magnetic susceptibility measured on groups of sediments. Studia Geoph. Geod. 22, 50–62.

Jelinek, V., 1981. Characterization of the magnetic fabric of rocks. Tectonophysics 79, 63–67.

Jiménez-Moreno, G., Rodríguez-Tovar, F.J., Pardo-Igúzquiza, E., Fauquette, S., Suc, J.P., Müller, P., 2005. High-resolution palynological analysis in late early–middle Miocene core from the Pannonian Basin, Hungary: climatic changes, astronomical forcing and eustatic fluctuations in the Central Paratethys. Palaeogeogr. Palaeoclimatol. Palaeoecol. 216, 73–97.

Karátson, D., Márton, E., Sz, Harangi, Józsa, S., Balogh, K., Pécskay, Z., Kovácsvölgyi, S., Gy, Szakmány, Dulai, A., 2000. Volcanic evolution and stratigraphy of the Miocene Börzsöny Mountains, Hungary: an integrated study. Geol. Carpath. 51, 325–343.

Karátson, D., Oláh, I., Pécskay, Z., Márton, E., Harangi, Sz, Dulai, A., Zelenka, T., Kósik, Sz, 2007. Miocene volcanism in the Visegrád Mountains (Hungary): an integrated approach to regional volcanic stratigraphy. Geol. Carpath. 58, 541–563.

Kataoka, K., 2003. Volcaniclastic remobilization and resedimentation in distal terrestrial settings in response to large-volume rhyolitic eruptions: examples from the Plio-Pleistocene volcaniclastic sediments, central Japan. J. Geosci. 46, 47–65.

Kataoka, K., Nakajo, T., 2002. Volcaniclastic resedimentation in distal fluvial basins induced by large-volume explosive volcanism: the Ebisutoge–Fukuda tephra, Plio-Pleistocene boundary, central Japan. Sedimentology 319–334.

Koněcný, V., Lexa, J., Hojstričová, V., 1995. The Central Slovakian volcanic field: a review. Acta Vulcanol. 7, 63–78.

Koněcný, V., Kováč, M., Lexa, J., Šefara, J., 2002. Neogene evolution of the Carpatho-Pannonian region: an interplay of subduction and back-arc diapiric uprise in the mantle. EGU Stephan Muller Special Publ. Ser. 1, 105–123.
Kováč, M., Andreyeva-Grigorovich, A., Bajraktarevic, Z., Brzobohatý, R., Filipescu, S., Fodor, L., Harzhauser, M., Nagymarosy, A., Oszczypko, N., Pavelic, D., 2007. Badenian evolution of the Central Paratethys Sea: paleogeography, climate and eustatic sea-level changes. Geol. Carpath. 58, 579–606.
Kováč, M., Hudáčková, N., Halásová, E., Kováčová, M., Holcová, K., Oszczypko-Clowes, M., Báldi, K., Less, G., Nagymarosy, A., Ruman, A., Klučiar, T., 2017. The Central Paratethys palaeoceanography: a water circulation model based on microfossil proxies, climate, and changes of depositional environment. Acta Geologica Slovaca 9, 75–114.
Kovács, I., Szabó, Cs, 2008. Middle Miocene volcanism in the vicinity of the Middle Hungarian zone: evidence for an inherited enriched mantle source. J. Geodyn. 45, 1–15.
Kovács, I., Csontos, L., Szabó, C.S., Falus, G.Y., Bali, E., Benedek, K., Zajacz, Z., 2007. Paleogene-Early Miocene volcanic rocks and geodynamics of the Alpine-Carpathian Pannonian-Dinaric region: an integrated approach. In: Beccaluva, L., Bianchini, G., Wilson, M. (Eds.), Cenozoic Volcanism in the Mediterranean Area. Geol. Soc. of Am. Spec. Paper. vol. 418, pp. 93–112.
Lirer, L., Pescatore, T., Booth, B., Walker, G.P.L., 1973. Two Plinian Pumice-fall deposits from Somma-Vesuvius, Italy. Bull. Geol. Soc. Am. 84, 759–772.
Liu, E., Cashman, K., Rust, A., 2015. Optimising shape analysis to quantify volcanic ash morphology. Geo. Res. J. 8, 14–30.
Lukács, R., Harangi, Sz, Ntaflos, T., Koller, F., Pécskay, Z., 2007. The characteristics of the Upper Rhyolite Tuff Horizon in the Bükkalja Volcanic Field: the Harsány ignimbrite unit. Földt. Közl. (Bull. Hung. Geol. Soc.) 137, 487–514 (in Hungarian with English abstract and figure captions).
Lukács, R., Harangi, Sz, Radóc, Gy, Kádár, M., Pécskay, Z., Ntaflos, T., 2010. The Miocene pyroclastic rocks of the boreholes Miskolc–7, Miskolc–8 and Nyékládháza–1 and their correlation with the ignimbrites of Bükkalja. Földt. Közl. (Bull. Hung. Geol. Soc.) 140, 31–48 (in Hungarian with English abstract and figure captions).
Lukács, R., Harangi, Sz., Bachmann, O., Guillong, M., Danisik, M., Buret, Y., von Quadt, A., Dunkl, I., Fodor, L., Sliwinski, J., Soós, I., Szepesi, J., 2015. Zircon geochronology and geochemistry to constrain the youngest eruption events and magma evolution of the Mid-Miocene ignimbrite flare-up in the Pannonian Basin, eastern-central Europe. Contrib. Mineral. Petr. 170, 1–26.
Lukács, R., Harangi, Sz., Guillong, M., Bachmann, O., Fodor, L., Buret, Y., Dunkl, I., Sliwinski, J., von Quadt, A., Peytcheva, I., Zimmerer, M., 2018. Early to Mid-Miocene syn-extensional massive silicic volcanism in the Pannonian Basin (East-Central Europe): eruption chronology, correlation potential and geodynamic implications. Earth Sci. Rev. 179, 1–19.
Manville, V., Wilson, C.J.N., 2004. The 26.5 ka Oruanui eruption, New Zealand: a review of the roles of volcanism and climate in the post-eruptive sedimentary response. New Zeal. J. Geol. Geop. 47, 525–547.
Márton, E., Fodor, L., 1995. Combination of palaeomagnetic and stress data—a case study from North Hungary. Tectonophysics 242, 99–114.
Márton, E., Fodor, L., 2003. Tertiary paleomagnetic results and structural analysis from the Transdanubian Range (Hungary): rotational disintegration of the Alcapa unit. Tectonophysics 363, 201–224.
Márton, E., Márton, P., 1996. Large scale rotations in North Hungary during the Neogene as indicated by paleomagnetic data. In: Morris, A., Tarling, D.H. (Eds.), Paleomagnetism and Tectonics of the Mediterranean Region. Geol. Soc. Spec. Publ. vol. 105. United Kingdom, London, pp. 153–173.
Márton, E., Pécskay, Z., 1998. Complex evaluation of paleomagnetic and K/Ar isotope data of the Miocene ignimbritic volcanics in the Bükk Foreland, Hungary. Acta Geol. Hungar. 41, 467–476.
Márton, E., Márton, P., Zelenka, T., 2007. Paleomagnetic correlation of Miocene pyroclastics of the Bükk Mts and their forelands. Cent. Eur. Geol. 50, 47–57.
McPhie, J., 1986. Primary and redeposited facies from a large magnitude, rhyolitic, phreatomagmatic eruption: Cana Creek Tuff, late Carboniferous, Australia. J. Volcanol. Geotherm. Res. 28, 319–350.
Morrissey, M.M., Zimanowski, B., Wohletz, K., Buettner, R., 2000. Phreatomagmatic fragmentation. In: Sigurdsson, H., Houghton, B., McNutt, S., Rymer, H., Stix, J. (Eds.), The Encyclopedia of Volcanoes, First edition Academic Press, San Diego, USA, pp. 431–445.
Mueller, S.B., Kueppers, U., Ametsbichler, J., Cimarelli, C., Merrison, J.P., Poret, M., Wadsworth, F.B., Dingwell, D.B., 2017. Stability of volcanic ash aggregates and break-up processes. Sci. Rep. 7, 7440.
Németh, K., Kósik, S., 2020. Review of explosive hydrovolcanism. Geosciences 10, 44.
Ort, M.H., Orsi, G., Pappalardo, L., Fisher, R.V., 2003. Anisotropy of magnetic susceptibility studies of depositional processes in the Campanian Ignimbrite, Italy. Bull. Volcanol. 65, 55–72.
Ort, M.H., Newkirk, T.T., Vilas, J.F., Vazquez, J.A., 2015. Towards the definition of AMS facies in the deposits of pyroclastic density currents. In: Ort, M.H., Porreca, M., Geissman, J.W. (Eds.), The Use of Palaeomagnetism and Rock Magnetism to Understand Volcanic Processes. Geol. Soc. Spec. Pub. vol. 396. United Kingdom, London, pp. 205–226.
Palladino, D.M., Taddeucci, J., 1998. The basal ash deposit of the Sovana Eruption (Vulsini Volcanoes, central Italy): the product of a dilute pyroclastic density current. J. Volcanol. Geotherm. Res. 87, 233–254.
Pantó, G., 1962. The role of ignimbrites in the volcanism of Hungary. Acta Geol. Hung. 6, 307–331.
Pantó, G., 1965. Miozäne Tuffhorizonte Ungarns. Acta Geol. Hung. 9, 225–233 (in German with English abstract).
Pécskay, Z., Lexa, J., Szakács, A., Balogh, K., Seghedi, I., Konečný, V., Kovács, M., Márton, E., Kaliciak, M., Széky-Fux, V., Póka, T., Gyarmati, P., Edelstein, O., Rosu, E., Zec, B., 1995. Space and time distribution of Neogene-Quaternary volcanism in the Carpatho-Pannonian region. In: Downes, H., Vaselli, O. (Eds.), Neogene and Related Magmatism in the Carpatho-Pannonian Region. Acta Vulcanologica. vol. 7, pp. 15–28.
Pécskay, Z., Lexa, J., Szakács, A., Seghedi, I., Balogh, K., Konečný, V., Zelenka, T., Kovács, M., Póka, T., Fülöp, A., Márton, E., Panaiotu, C., Cvetkovic, V., 2006. Geochronology of Neogene magmatism in the Carpathian arc and intra-Carpathian area. Geol. Carpath. 57, 511–530.
Piller, W.E., Harzhauser, M., Mandic, O., 2007. Miocene Central Paratethys stratigraphy - current status and future directions. Stratigraphy 151–168.
Póka, T., Zelenka, T., Szakács, A., Seghedi, I., Nagy, G., Simonits, A., 1998. Petrology and geochemistry of the Miocene acidic explosive volcanism of the Bükk Foreland; Pannonian Basin, Hungary. Acta Geol. Hung 41, 437–466.
Porreca, M., Mattei, M., Giordano, G., De Rita, D., Funicielo, G., 2003. Magnetic fabric and implications for pyroclastic flow and lahar emplacement, Albano maar, Italy. J. Geophys. Res.-Earth 108, 1–14.
Porreca, M., Mattei, M., MacNiocaill, C., Giordano, G., McClelland, E., Funiciello, R., 2008. Paleomagnetic evidence for low-temperature emplacement of the phreatomagmatic Peperino Albano ignimbrite (Colli Albani volcano, Central Italy). Bull. Volcanol. 70, 877–893.
Ravasz, Cs, 1987. Neogene volcanism in Hungary. Ann. Inst. Geol. Publ. Hung. 70, 275–279.
Rochette, P., 1987. Magnetic susceptibility of the rock matrix related to the magnetic fabric studies. J. Struct. Geol. 9, 1015–1020.
Rochette, P., Jackson, M., Aubourg, C., 1992. Rock magnetism and the interpretation of anisotropy of magnetic susceptibility. Rev. Geophys. 30, 209–226.
Scarpati, C., Cole, P., Perrotta, A., 1993. The Neapolitan Yellow Tuff – a large volume multiphase eruption from Campi Flegrei, southern Italy. Bull. Volcanol. 55, 343–356.
Scasso, R.A., Corbella, H., Tiberi, P., 1994. Sedimentological analysis of the tephra from the 12–15 August 1991 eruption of Hudson volcano. Bull. Volcanol. 56, 121–132.
Schumacher, R., Mues-Schumacher, U., 1997. The pre-ignimbrite (phreato) plinian and phreatomagmatic phases of the Akdag-Zelve ignimbrite eruption in Central Anatolia, Turkey. J. Volcanol. Geotherm. Res. 78, 139–153.
Schumacher, R., Schmincke, H.U., 1991. Internal structure and occurrence of accretionary lapilli – a case study at Laacher See Volcano. Bull. Volcanol. 53, 612–634.
Scolamacchia, T., Macías, J.L., Sheridan, M.F., Hughes, S.R., 2005. Morphology of ash aggregates from wet pyroclastic surges of the 1982 eruption of El Chichón Volcano, Mexico. Bull. Volcanol. 68, 171–200.
Scott, W.E., Hoblitt, R.P., Torres, R.C., Self, S., Martinez, M.M.L., Nillos, T., 1996. Pyroclastic Flows of the June 15, 1991, Climactic Eruption of Mount Pinatubo. Fire and Mud: Eruptions and Lahars of Mount Pinatubo, Philippines. pp. 545–570.
Seghedi, I., Downes, H., Szakács, A., Mason, P.R.D., Thirlwall, M.F., Rosu, E., Pécskay, Z., Márton, E., Panaiotu, C., 2004. Neogene–Quaternary magmatism and geodynamics in the Carpathian-Pannonian region: a synthesis. Lithos 72, 117–146.
Self, S., 1983. Large scale silicic phreatomagmatic volcanism: a case study from New Zealand. J. Volcanol. Geotherm. Res. 17, 433–469.
Self, S., Sparks, R.S.J., 1978. Characteristics of widespread pyroclastic deposits formed by the interaction of silicic magma and water. Bull. Volcanol. 41, 196–212.
Shoji, D., Noguchi, R., Otsuki, S., Hino., H., 2018: Classification of volcanic ash particles using a convolutional neural network and probability. Sci. Rep., 8:8111 DOI:https://doi.org/10.1038/s41598-018-26200-2.
Sparks, R.S.J., Wilson, L., Sigurdsson, H., 1981. The pyroclastic deposits of the 1875 Askja, Iceland. Philos. Trans. R. Soc. London 299, 241–273.
Smith, G.A., Katzman, D., 1991. Discrimination of eolian and pyroclastic-surge processes in the generation of cross-bedded tuffs, Jemez Mountains volcanic field, New Mexico. Geology 19, 465–468.
Szabó, Cs, Harangi, Sz, Csontos, L., 1992. Review of Neogene and Quaternary volcanism of the Carpathian–Pannonian region. Tectonophysics 208, 243–256.
Szakács, A., Márton, E., Póka, T., Zelenka, T., Pécskay, Z., Seghedi, I., 1998. Miocene acidic explosive volcanism in the Bükk Foreland, Hungary: identifying eruptive sequences and searching for source locations. Acta Geol. Hung. 41, 413–435.
Szakács, A., Pécskay, Z., Silye, L., Balogh, K., Vlad, D., Fülöp, A., 2012. On the age of the Dej Tuff, Transylvanian Basin (Romania). Geol. Carpath. 63, 139–148.
Szakács, A., Pécskay, Z., Gál, Á., 2018. Patterns and trends of time–space evolution of Neogene volcanism in the Carpathian–Pannonian region: a review. Acta Geod. Geophys. HU. 53, 347–367.
Széky-Fux, V., Pécskay, Z., Balogh, K., 1987. Miocene volcanic rocks from boreholes in Transtibiscia (Hungary) and their K/Ar chronology. Bull. Acad. Serbe Sci. Arts Classe Sci. Nat. 92, 109–128.
Talbot, J.P., Self, S., Wilson, C.J.N., 1994. Dilute gravity current and rain-flushed ash deposits in the 1.8 ka Hatepe Plinian deposit, Taupo, New Zealand. Bull. Volcanol. 56, 538–551.
Tarling, D., Hrouda, F., 1993. Magnetic Anisotropy of Rocks. Springer Science & Business Media.
Tilley, C.E., 1922. Density, refractivity, and composition relations of some natural glasses. Mineral. Mag. 96, 275–294.
Van Eaton, A.R., Wilson, C.J., 2013. The nature, origins and distribution of ash aggregates in a large-scale wet eruption deposit: Oruanui, New Zealand. J. Volcanol. Geotherm. Res. 250, 129–154.
Van Eaton, A.R., Herzog, M., Wilson, C.J.N., McGregor, J., 2012. Ascent dynamics of large phreatomagmatic eruption clouds: the role of microphysics. J. Geophys. Res. Solid Earth 117 (B3).
Van Eaton, A.R., Harper, M.A., Wilson, C.J., 2013. High-flying diatoms: Widespread dispersal of microorganisms in an explosive volcanic eruption. Geology 41, 1187–1190.
Vespa, M., Keller, J., Gertisser, R., 2006. Interplinian explosive activity of Santorini volcano (Greece) during the past 150,000 years. J. Volcanol. Geotherm. Res. 153, 262–286.
Vogel, S., Märker, M., Rellini, I., Hoelzmann, P., Wulf, S., Robinson, M., Steinhüberl, L., Di Maio, G., Imperatore, C., Kastenmeier, P., Liebmann, L., Esposito, D., Seiler, F., 2016.

From a stratigraphic sequence to a landscape evolution model: Late Pleistocene and Holocene volcanism, soil formation and land use in the shade of Mount Vesuvius (Italy). Quat. Int. 394, 155–179.
Walker, G.P.L., 1971. Grain-size characteristics of pyroclastic deposits. J. Geol. 79, 696–714.
Walker, G.P.L., 1973. Explosive volcanic eruptions – a new classification scheme. Geol. Rundsch. 62, 431–446.
Walker, G.P.L., 1981a. Characteristics of two phreatoplinian ashes, and their water-flushed origin. J. Volcanol. Geotherm. Res. 9, 395–407.
Walker, G.P.L., 1981b. Plinian eruptions and their products. Bull. Volcanol. 44, 223.
Walker, G.P.L., 1983. Ignimbrite types and ignimbrite problems. J. Volcanol. Geoth. Res. 17, 65–88.
Walker, G.P.L., Croasdale, R., 1971. Two Plinian-type eruptions in the Azores. J. Geol. Soc. 127, 17–55.
White, J.D.L., Valentine, G.A., 2016. Magmatic versus phreatomagmatic fragmentation: absence of evidence is not evidence of absence. Geosphere 12, 1478–1488.
Wilson, C.J.N., 1993. Stratigraphy, chronology, styles and dynamics of Late Quaternary eruptions from Taupo Volcano, New-Zealand. Phil. Trans. R. Soc. Lond. Series A - Mathematical Physical And Engineering Sciences 343, 205–306.
Wilson, C.J.N., 2001. The 26.5 ka Oruanui eruption, New Zealand: an introduction and overview. J. Volcanol. Geotherm. Res. 112, 133–174.
Wilson, C.J.N., Walker, G.P.L., 1985a. The Taupo eruption, New Zealand. I. General aspects. Phil. Trans. R. Soc. Lond. 314, 199–228.
Wilson, C.J.N., Walker, G.P.L., 1985b. The Taupo Eruption, New-Zealand. II. The Taupo Ignimbrite. Phil. Trans. R. Soc. Lond. 314, 229–310.
Wilson, C.J.N., Blake, S., Charlier, B.L.A., Sutton, A.N., 2006. The 26.5 ka Oruanui eruption, Taupo volcano, New Zealand: development, characteristics and evacuation of a large rhyolitic magma body. J. Petrol. 47, 35–69.
Zelenka, T., Balázs, E., Balogh, K., Kiss, J., Kozák, M., Nemesi, L., Pécskay, Z., Püspöky, Z., Ravasz, Cs., Széky-Fux, V., Újfalussy, A., 2004. Buried Neogene volcanic structures in Hungary. Acta Geol. Hung. 47, 177–219.